Nanocomposite of ZrO_2/Polymer Thin-Film Coatings by The Ionically Self-Assembled Monolayer Technique

by

Aprillya Rosidian

Thesis submitted to the Faculty of the
Virginia Polytechnic Institute and State University
in partial fulfillment of the requirements for the degree of
MASTER OF SCIENCE
In
Materials Science and Engineering

APPROVED:

Dr. Richard O. Claus, Chair

Dr. James R. Heflin

Dr. Ronald S. Gordon

March, 1998
Blacksburg, Virginia

Nanocomposite of ZrO_2/Polymer Thin-film Coatings by The Ionically Self-Assembled Monolayer Technique

by

Aprillya Rosidian

Dr. Richard O. Claus, Chairman
Department of Materials Science and Engineering
Virginia Polytechnic Institute and State University

(**ABSTRACT**)

Nanocomposites of multilayer structures of zirconia/polymer thin-film coatings have been fabricated on quartz and single-crystal silicon substrates by the Ionically Self-Assembled Monolayer (ISAM) technique. Particle size distribution was measured to calculate the grain diameter of the zirconia particles. UV/Vis spectroscopy and ellipsometry were used to characterize the ISAM technique. SEM and AFM were used to observe the microscopic structure of the multilayer structures. Some mechanical properties were characterized by adhesion, abrasion, and nano-hardness tests. It was shown that an important distinction of this novel technique over conventional coating processes is the fabrication of excellent molecular-level uniform films with precise control of film thickness at the Ångström-level at ambient temperature and pressure conditions. It was also shown the maximum Vickers microhardness of ZrO_2/polymer nanocomposite thin-film coatings prepared by this method was greater than 25 GPa.

Acknowledgements

First of all, I would like to sincerely thank my research advisor, Dr. Richard Claus, for his encouragement and support. I really appreciate the opportunity that he gave me to pursue my graduate degree under his guidance and to be a part of FEORC's family. I would also like to thank my committee members, Dr. Ronald S. Gordon and Dr. James R. Heflin, for their time and support.

My appreciation goes to Dr. Yanjing Liu and Dr. You-Xiong Wang for their guidance throughout my research. I thank them for the invaluable discussion and assistance in carrying out my research experiments.

To Steve McCartney of the Surface Imaging Laboratory at Virginia Tech, I thank him for his assistance with the AFM measurements. I also thank the Centre Suisse d'Electronique et de Microtechnique SA for the Vickers microhardness measurements.

Many thanks go towards the members of FEORC, past and present. I appreciate their friendship as well as their assistance in my research. Special thanks for Linda Jones who was very helpful and patient in taking care of every administrative work I needed.

I finally would like to thank my family and parents, Rosihan Inspiradi and Dian Angratih, for their moral support and encouragement. I am very grateful for all their love and inspiration.

This thesis is dedicated to my grandfather,
Inu Kertapati,
who passed away on January 30, 1998.

Table of Contents

List of Figures

List of Tables

Chapter 1

Introduction

During the past three decades, much scientific and engineering research has focused on the synthesis of nanophase materials. Nanophase materials contain building blocks of zero- to three-dimensional arrays of atoms with at least one dimension in the scale of less than 100 nanometers (1 nm = 10^{-9} m). It is anticipated that by arranging the atoms to form nanometer sized clusters, the properties of these nanophase materials will be different from, and often superior to, those of materials in their conventional bulk form.

Research has been conducted in the field of coating technology by manipulating the theory behind nanophase materials. Most coating applications use ceramics as coating materials because of their good thermal, mechanical, and chemical stability. Applications of thermal barrier coatings require materials that are able to withstand the high temperatures of operation. The materials also need to have good corrosion and oxidation resistance. Wear-resistant coatings require materials with good mechanical properties, such as hardness, strength, and fracture toughness. Materials with high refractive indices and low absorption coefficients would be good candidates for optical

coating applications. While meeting these requirements, good adhesion at the substrate-coating interface is also necessary.

Zirconia has long found use in coating technology because of its high strength, fracture toughness, chemical durability, thermal stability, high refractive index, and low optical absorption. One interesting property of zirconia is that it is polymorphic, which means that it possesses several crystal structures at different temperatures. With control of the martensitic transformation and grain size, one can design desired properties of zirconia for a specific coating application.

There are several methods available for the synthesis of zirconia thin-film coatings, some of which include sol-gel, spin coating, plasma spraying, electron beam evaporation, sputtering, and chemical vapor deposition (CVD) [1-2]. Prior studies have shown that problems exist in the fabrication of zirconia coatings. One serious problem in the plasma spraying technique is the presence of severe internal damage, such as macrocracks and microcracks, which degrade the mechanical properties of the coating. Films produced by the sol-gel technique have exhibited unmelted particles since a high melting temperature is required. Electron beam evaporation produces coatings with voids and columnar microstructures. Since it requires a control of many parameters, defects, such as non-uniformity, fracture, and incorporation of impurities into the coating layer, have been previously observed on coatings prepared by the CVD method [3]. All of these undesirable defects cause critical changes to the properties of coatings.

A new technique of layer-by-layer deposition of heterostructured multilayers containing oppositely charged monolayers has recently been employed in the synthesis of thin-films because of its ability to produce a dense and homogeneous film. This

technique is called the Ionically Self-Assembled Monolayer (ISAM), which is based on the self-assembly process [4-5]. Most recent applications of this technique have been in the fabrication of organic/organic and metal/organic thin-films [5-8]. However, with the advantage of control over the type and thickness of deposited layers and thin-film structures at the molecular level, fabrication of nanophase zirconia thin-film coatings becomes feasible.

The main goal of this study is to utilize the ISAM technique in the fabrication of zirconia thin-film coatings. Zirconia particle sizes were controlled to be below 100 nm by varying the concentrations. Different characterization techniques were performed to investigate any change in the structure or properties of the coating. Microscopy techniques of SEM (Scanning Electron Microscopy) and AFM (Atomic Force Microscopy) were employed to study the grain distributions of the monolayer coating. Particle size distributions were measured to see the distribution of sizes on the monolayer, and the thickness of the monolayer was measured by ellipsometry. Quantitative investigation of the optical properties was performed using UV/Vis spectroscopy. Adhesion and abrasion tests were performed to study the durability of the coating. Finally, hardness was measured to check for any improvement in mechanical properties.

Chapter 2

Nanophase Materials

2.1. Introduction

The idea of nanophase materials was first introduced in 1959 by Nobel laureate, Richard P. Feynman [9]. In his famous lecture, "There's Plenty of Room at the Bottom," Feynman described the possibility of manipulating atoms or molecules to create materials with new properties. However, the fabrication of nanophase materials was not initiated until the early 1980s [10-11].

Nanophase materials represent a new class of synthesized materials from zero to three dimensional microstructures with an average grain size or other structural domain size less than 100 nanometers (1 nm = 10^{-9} m) [10, 12]. The wide range of nanophase materials, shown in Figure 2.1, includes zero-dimensional materials, one-dimensional multilayers, two-dimensional ultrafine-grained overlayers, coatings, or buried layers, and three-dimensionally modulated analogous nanophase materials [8, 10, 12-13]. One unique characteristic of this new class of materials is that a significant fraction of their

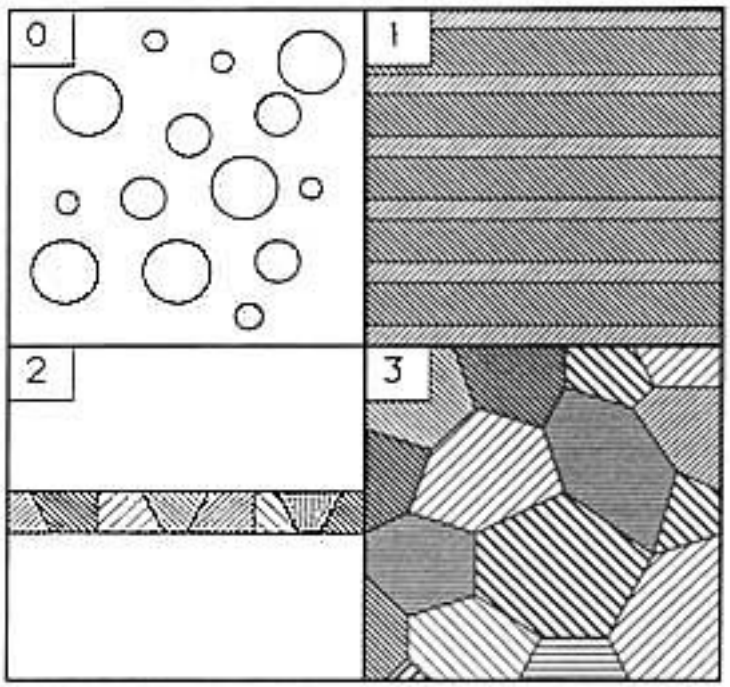

Figure 2.1. The schematic diagrams of the four types of nanophase materials, classified according to integral modulation dimensionality, from zero, in a, to three, in d. a: Clusters of any aspect ratio from 1 to infinity. b: Multilayers. c: Ultrafine-grained overlayers, coatings, or buried layers. d: Nanophase materials [10].

atoms reside at the grain boundaries. Nanophase materials can have as much as 50% of their atoms at the grain boundaries, where conventional polycrystalline materials typically have less than 1% [10, 14]. This atomic arrangement characteristic of nanophase materials leads to improvements in many physical properties, such as wear resistance, strength, and hardness [10]. Thus, all types of nanophase materials share three important fundamental features: atomic domains spatially confined to less than 100 nm (grains, layers, or phases), significant atom fractions associated with interfacial environments, and interactions between their constituent domain, that determine their unique properties [10, 12, 15].

The idea of fabricating composites of nanophase materials opens new opportunities to create infinite arrangements of desirable properties for specific applications [10, 16]. There are several broad categories of nanocomposites that are being studied. They include ceramic/ceramic, metal/ceramic, metal/metal, ceramic/polymer, and combinations of other organic and inorganic materials [16]. Research in nanocomposites offers many extended promising research opportunities for the industrial community.

2.2. Synthesis and Processing

The synthesis and processing of nanophase materials play important roles in controlling desired properties. There are numerous methods used to synthesize nanophase materials, some of which include chemical or physical vapor deposition, gas-condensation, self-assembly, and chemical precipitation. These techniques manipulate

the atoms or molecules on the microscopic level and give more capacity of alternating material properties [15]. Other methods are also available from processing of bulk precursors, such as mechanical attrition, crystallization from the amorphous state, and phase separation. A more comprehensive discussion of these methods is described elsewhere [10].

There are three crucial aspects of synthesizing nanophase materials based on the fundamental features that they possess [10]. The first aspect is the control of size and size distribution. To achieve a dramatic increase in properties, the grain size must be below 100 nanometers. At this scale, the properties of materials begin to change dramatically because of a variety of confinement effects. It is also important to obtain uniform size distribution avoiding anisotropy. The second aspect is the control of compositions of the constituent phases in a nanophase material. Control of the composition of the constituent phases means maintaining phase purity during synthesis in single-phase materials, such as oxides or metals. It can also mean controlling the impurity doping level, the stoichiometries, the solute gradients, the phase mixtures, or combinations of these in more complex nanophase materials [12]. The third aspect is the nature of the interfaces created between constituent phases and the nature of the interactions across the interface.

The design of distinct properties depends on manipulations of the processing characteristics (domain size, composition, and interface interactions). In some specific applications, one or more of these features may dominate [10]. Therefore, it is possible to have a controllable process, which will tailor a material with specific properties.

2.3. Structures and Properties

The structures and properties of nanophase materials are expected to be different from their conventional coarser-grained polycrystalline forms. The way the atoms are arranged determines the changes in the properties. This manipulation of the atomic arrangement plays a very important role in the resulting material properties. The properties are dominated by ultrafine grain sizes, the compositions, and the large number of associated interfaces. In addition, other structural features, such as pores (and larger flaws), grain-boundary junctions, and other crystal-lattice defects affect the properties of materials significantly [12]. It has become increasingly clear that all of these structural aspects of nanophase materials must be considered in trying to fully understand the properties of these new materials.

Because of their ultrafine grains, a large fraction of their atoms resides at their grain boundaries. For example, as shown in Figure 2.2, nanophase materials with a grain diameter of 5 nm, assuming the average grain boundary thickness is 1.0 nm (*i.e.*, about four nearest-neighbor distances in a metal), will have nearly 50% of their atoms residing at the grain boundaries. Materials with a grain diameter of 10 nm will have approximately 30%, and only 3% for 100 nm grain size materials. Thus, the properties of this new class of materials will be strongly affected by the nature of their interface structure, because of the high density in the boundaries and significant fraction of atoms associated with them [14].

Further investigations by Gleither and co-workers on the interface structure of metals showed that the grains in nanophase materials are arranged randomly, adopting neither the short-range nor the long-range order normally found in the conventional form

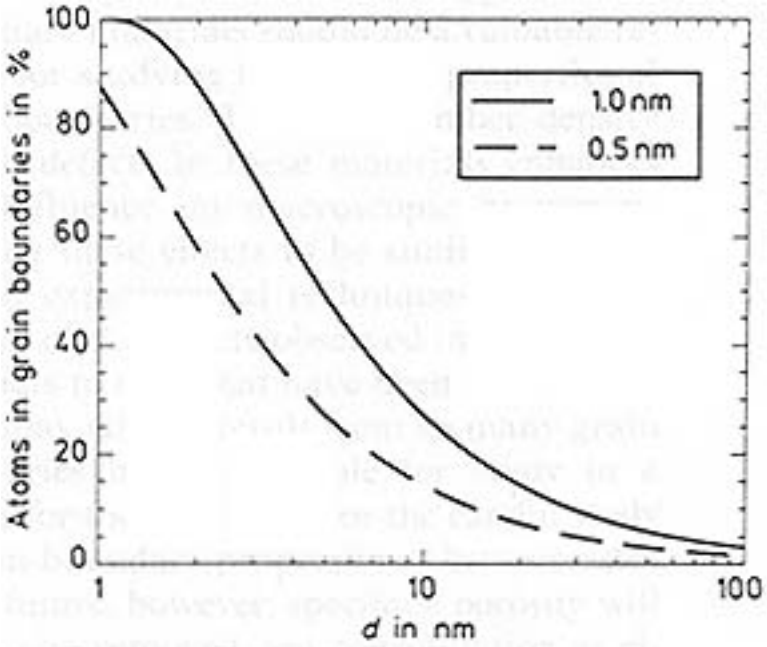

Figure 2.2. Range of percentage of atoms in grain boundaries of a nanophase material as a function of grain diameter, assuming that the average grain boundary thickness ranges from 0.5 to 1.0 nm (ca 2 to 4 atomic planes wide) [10].

of metals [10]. Observations by both electron and x-ray scattering indicate that there is no apparent preferred crystallographic orientations or texture of the grain resulting from synthesis.

Surface interactions have been proven to be more reactive than bulk interactions. A large proportion of the atoms of nanophase materials in the grain boundaries could react with each other rather aggressively, even at low temperatures [10]. Studies of nanophase titanium oxide (TiO_2) showed that this material sintered at temperatures 400°C to 600°C, lower than that of the conventional TiO_2 form. Furthermore, doping the TiO_2 with yttrium reduced the sintering temperature without sacrificing the formation of ultrafine-grain TiO_2 [12].

Although synthesis of nanophase materials typically produces structures with a high packing density, characterization with positron annihilation spectroscopy (PAS) indicated the presence of porosity in these materials. The detected porosity ranges from about 25% to less than 5%, which is generally smaller for metals and higher for ceramics. Most of the porosity observed in the studies was primarily smaller than or equal to the grain size of the materials, however, larger porous flaws have been observed using optical and scanning electron microscopy [10]. Control and removal of this defect could be done during fabrication at low temperature, thus retaining the ultra fine grain sizes in these materials [10, 12].

Atomic diffusion in nanophase materials has been found to be very rapid, several magnitudes larger than in their coarser grain counterparts [10]. Because nanophase materials have a very large fraction of their atoms in the grain boundaries, the grain boundary diffusion mechanism plays an important role in the mechanical properties of

these materials [14]. Taking advantage of both porosity and enhanced diffusion mechanisms in nanophase materials allows the possibility of embedding atoms of different properties into the nanophase matrix, thus synthesizing materials with tailored chemical, mechanical, or other physical properties [10, 14].

An increase in hardness or strength has been the major improvement in mechanical properties of nanophase materials. It is anticipated from the Hall-Petch strengthening mechanism that as the grain size decreases, the hardness of a material increases [17]. However, other mechanisms can account for this enhancement as well. Metals, in their conventional form, are ductile, due to the very easy multiplication and movement of dislocations through their crystal lattice [10, 12]. Nanophase metals will be significantly harder in comparison to conventional metals because there is no dislocation available to operate when their grain size falls below the critical length for the mechanism [10, 12, 18]. The representation of Frank-Read dislocation multiplication is shown in Figure 2.3. As the grain size is reduced, the dislocation generation and migration of easier mechanisms will be frozen out, requiring higher energy for the deformation mechanism to operate [10]. Thus, spatial confinement that leads to a highly compacted structure results in substantial enhancement of the mechanical properties of the nanophase materials.

Ceramics, however, demonstrate behavior opposite to that of metals. In their nanophase form, ceramics are easily formed. This tendency toward increased ductility is apparently an intrinsic property of these nanophase ceramics [10, 12, 15, 18]. A grain boundary sliding mechanism proposes that atoms are able to slide from one lattice point to another. This is because of their ultrafine grain size in conjunction with the presence

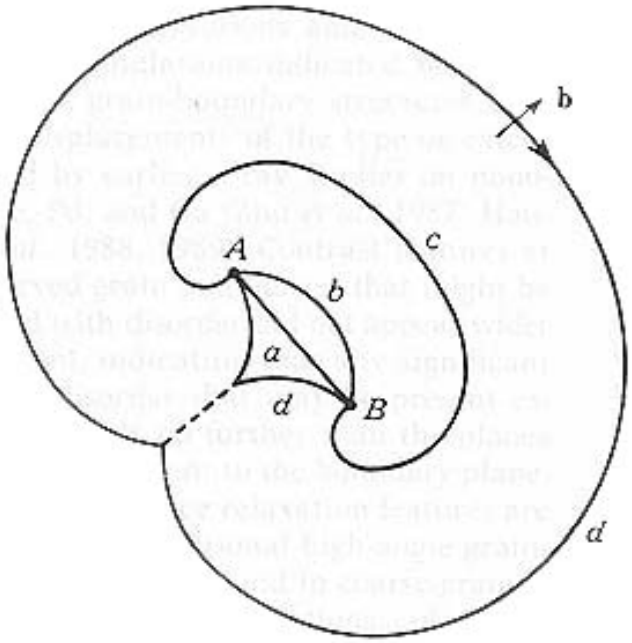

Figure 2.3. Schematic representation of a Frank-Read dislocation multiplication. A segment of dislocation loop a of length L and Burgers vector b is pinned between points A and B in a material of shear modulus G. When the stress applied to the dislocation line segment exceeds a critical stress, $\sigma_{crit} = kGb/L$, the dislocation bows out ($a \rightarrow b \rightarrow c \rightarrow d$) until it creates a new dislocation loop. The constant of proportionality, k, is 0.5 for an edge dislocation and 1.5 for a screw dislocation [10].

of porosity and rapid short-range diffusion [7, 12, 15]. The increase in ductility of nano ceramics depends on the interfaces of these materials. The necessary presence of porosity allows the atoms to slide without fracturing the sample [12, 18]. Extrapolating from this behavior, one can expect that grain boundary sliding mechanisms, accompanied by short-range diffusion-assisted healing events, would dominate, therefore increasing the deformation of a wide range of nanophase materials [12, 18].

2.4. Applications of Multilayered Nanophase Materials

Among the various nanostructures, multilayered materials have the longest history. Applications of these nanostructures have already been seen in semiconductor devices, magnetic multilayer, and nonlinear optoelectronic devices [13]. Other applications of nanoscale multilayers include protective coatings, such as thermal barriers and ultrahard or wear-resistant coatings. By building a structure with several layers of nanophase materials, it is anticipicated that the resistance to corrosion and abrasion will be enhanced while retaining a dense and homogeneous coating structure.

Chapter 3

Self-Assembly Process

3.1. Langmuir-Blodgett Films

The Langmuir-Blodgett process (LB) has been widely used as a deposition technique for organic materials to create multilayer films [19-21]. The technique was initiated by Langmuir in 1920, however, it was not developed until 1935 when Katherine Blodgett successfully performed multilayer deposition of carboxylic acids on a solid substrate from an air-water interface [19-21]. Since then, further research has been conducted to gain a better understanding of this technique.

The technique of LB deposition is based on oil and water theory. There are three types of LB deposition as seen in Figure 3.1. The LB technique makes use of amphiphilic molecules (*i.e.,* molecules which have both a hydrophilic head and hydrophobic tail). The bonding between the hydrophobic ends of the molecules in a multilayer consists almost entirely of van der Waals interaction [22]. However, the bonding between the hydrophilic ends is far less understood [19-21].

The main characteristic of LB deposition is the ability to deposit ordered multilayers of organic molecules such that the number of layers is precisely known [19-

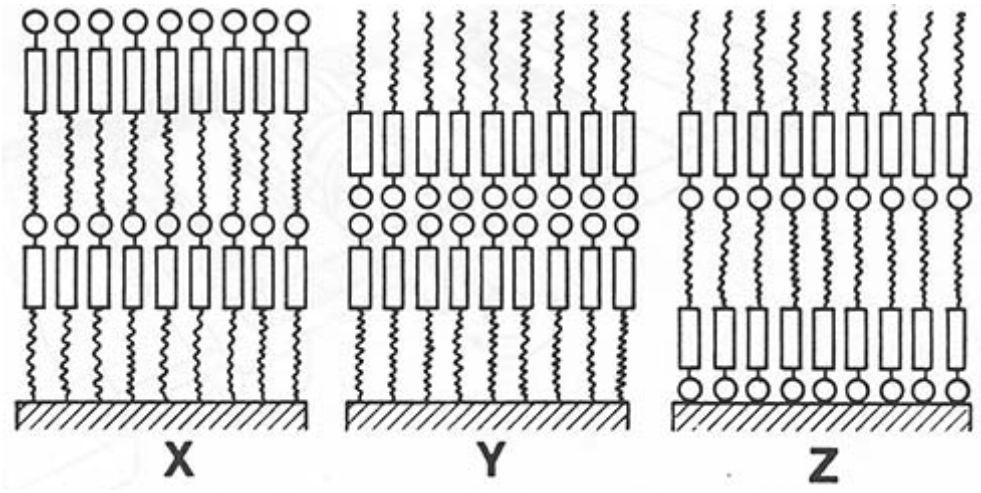

Figure 3.1. The common deposition mode for classical LB films is Y-type, where the molecules stack vertically with a head to head and tail to tail configuration. However, X and Z-type depositions are also observed [20].

21]. Because of this interesting feature, LB deposition has found its way in a very broad range of applications, such as electronics, chemistry, physics, and materials science.

3.2. Ionically Self-Assembled Monolayer (ISAM) Process

The concept behind self-assembly processes was inspired by nature. A raindrop will assume a particular shape spontaneously to minimize the area of an unstable surface [23]. Living cells as they duplicate themselves will direct their functions inside the cells. A self-assembly process is one where human involvement is eliminated. The idea of a process in which atoms or molecules will complimentarily rearrange themselves into a beneficial arrangement is very attractive.

The basic principle of the self-assembly process is selective stickiness. If two different molecular parts have complimentary structures or charges (*i.e.*, one has a hollow and the other has a bump, or one has a positive charge and the other has a negative charge), when mixed together, they will rearrange themselves in the simplest particular way to form a bigger part [24]. Thus, this bigger part can combine with its other complimentary bigger part in the same way to form a complex whole.

To assist in the complexity of rearranging atoms in a microscopic scale, the self-assembly process becomes a potential tool for fabrication of nanophase materials. There are two different self-assembly processes that are used in the fabrication of monolayers. The first process is self-assembly monolayers by chemisorptions (SAMs). This process involves the formation of chemical bonding between the monolayers in the multilayered structure. This technique sometimes requires several chemical activation steps, thus the

multilayer buildup can become a time consuming procedure [6]. The second process is the self-assembly of monolayers by physisorption (SAMp) [22]. There is no chemical reaction involved in this process. Most of the connections between monolayers rely on weaker and less directional bonds, such as ionic, hydrogen, or van der Waals forces [8].

Ionically self-assembled monolayer (ISAM) has been successfully developed by G. Decher and his coworkers, based on the SAMp methods. This technique utilizes the attraction of oppositely charged molecules of anionic and cationic polyelectrolytes in aqueous forms [4, 7]. The motivation behind the exploration of this technique was in the hope of fabricating ultrathin organic films that consist of large numbers of molecules of varying structures and properties to create a tailor-made system for a specific scientific or technology application [5, 7]. The construction of a multilayer structure by this means is very efficient and the process allows detailed structural control at the molecular level with ease of manufacturing.

One important advantage of the ISAM technique is that there is no substrate size limitation since the deposition is done by adsorption of individual layers from solutions [5, 7]. The ISAM process, shown in Figure 3.2, involves the alternate dipping of a charged substrate into an aqueous solution of the oppositely charged ions at room temperature. By then dipping the substrate in oppositely charged solution in a cyclic fashion, alternating multilayer assemblies can be obtained [4-5, 7].

Another advantage of the ISAM technique is the possibility of building composite multilayer structures. The process only requires two oppositely charged particles. Consequently, deposition of more than two kinds of oppositely charged molecules is

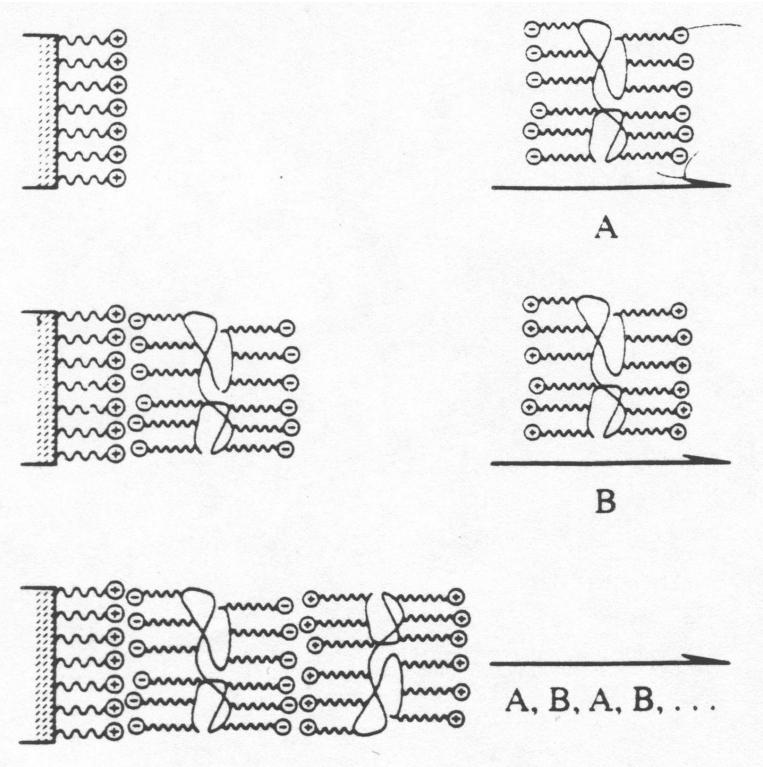

Figure 3.2. Schematic for the buildup of multilayer assemblies by ISAM [4].

feasible. Thus, one can simply immerse the substrate in as many solutions of polyelectrolytes as desired, as long as the charge is reversed from layer to layer [7].

Various materials with anisotropic, isotropic, or graded properties can be produced by this spontaneous layer-by-layer self-assembly technique to yield a wide range of new heterostructured materials. Furthermore, selecting the appropriate materials will lead to fabrication of nanophase materials with tailored mechanical, physical, chemical, or optical properties [6].

Chapter 4

Fabrication of Zirconia Thin-Film Coatings by the Ionically Self-Assembled Monolayer (ISAM) Method

4.1. Introduction

The development of new hard coating ceramics with higher toughness and ductility may lead to many applications in engines, machine, tools, and other wear-resistant components. The criteria for selecting the coating materials depend on the substrate to be used as well as the applications. Understanding the relationship between the manufacturing route, microstructure, defects, and properties allows appropriate coating applications [25].

Zirconia is one of the leading candidate materials for protective nanocluster coatings. It has promising characteristics such as high strength, fracture toughness, and abrasion resistance, as well as good chemical durability and thermal stability. Several different methods for the fabrication of zirconia thin-films are commonly employed. Physical vapor deposition, plasma spraying, and chemical processing are among the most commonly used methods. [1].

In this chapter the fabrication of zirconia nanoparticle coatings by the Ionically Self-Assembled Monolayer (ISAM) method is developed. This method allows for the fabrication of dense, homogeneous thin-films with improved properties. Specifically, the present work has shown that zirconia nanocluster thin-films prepared in this way have higher hardness values in comparison to zirconia films prepared by other methods.

The ISAM method has received attention as a simple fabrication procedure for the synthesis of multilayer architectures seen in nanophase materials. This method allows for detailed control over the film composition and thickness. The use of polyelectrolytes that provide alternating electrostatic attractions between layers offers significant advantages for the fabrication of multilayer films with reduced defect formation [6]. Individual layer thicknesses can be controlled by changes in ionic strength, pH, and molecular concentration. In addition, there are advantages in the low cost of fabrication instrumentation and high throughput of layer fabrication in comparison with previous techniques.

4.2. Experiments

4.2.1. Materials

Poly(allylamine hydrochloride) (PAH) (MW = 50,000 - 65,000) and poly(sodium-4-styrenesulfonate) (PSS) (MW = 70,000) were obtained from Aldrich Chemical Company, Inc. A molecular dye consisting of a poly(vinylamine) backbone with azo chromophores in the side chains (PS119) (MW = 100,000 – 160,000) was obtained from Sigma Chemical Company. Chemical structure representations of the organic materials

are shown in Figure 4.1. Zirconia nanocluster solution (formula weight = 23.22) was obtained from Alfa Aesar (20 wt.% ZrO_2 in H_2O; colloidal dispersion). NaCl and hydrochloric acid (HCl) were obtained from Fisher Scientific. Concentrated sulfuric acid (H_2SO_4) was obtained from Mallinkrodt. Hydrogen peroxide (H_2O_2) was obtained from Aldrich (30-32 wt.% solution in H_2O). The ultrapure water used for all experiments and for all cleaning steps was obtained from a Barnstead Nanopure III system. The resistivity of the water was above 17 MΩ/cm. All of these materials were used without further purification.

The substrates used in this study were quartz slides and silicon wafers. The quartz slides were purchased from Chemglass, Inc. at Virginia Tech and single crystal silicon (100) wafers were purchased from EL-CAT, Inc.

4.2.2. Experimental Procedures

4.2.2.1. Substrate Cleaning/Pre-treatment

Prior to any deposition, the substrates of quartz and silicon (100) wafers used in the study were cleaned to remove any impurities and, at the same time, to modify the surface charge. The substrates were immersed in a solution of H_2O_2 and concentrated H_2SO_4 mixture of 3:7 volume ratio at ambient laboratory temperature for about 30 minutes. Following the immersion, the substrates were rinsed extensively with deionized water and dried in an oven at 80°C for about 1 hour. This pre-treatment modified the surface of the substrates and made them negatively charged. The pre-treatment reaction is shown in Figure 4.2.

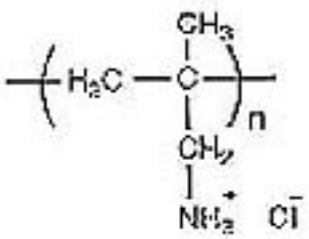

(PAH)

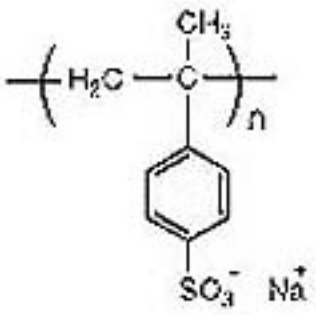

(PSS)

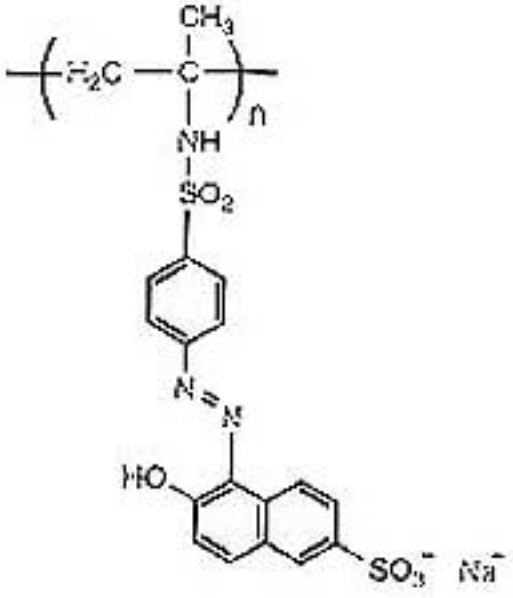

(PS119)

Figure 4.1. Chemical structures of the polyelectrolytes used in the fabrication of ZrO_2/polymer nanocomposite thin-films.

Figure 4.2. Pre-treatment reaction to modify the surface charge of quartz or silicon substrates.

4.2.2.2. Solution Preparation

Solutions of PAH were prepared by dissolving the polymer (50 mg) in deionized water (25 ml). NaCl (25 mg) was added to the solution that was continuously stirred for 10 minutes. The PS119 solution was prepared following the same procedure, except that the solution was stirred for a longer time (3 hours). The PAH and PS119 solutions were used as the cationic and anionic polyelectrolytes, respectively.

Solutions of PSS were prepared by dissolving the polymer (200 mg) in deionized water (100 ml), followed by the addition of NaCl (100 mg). The solution was stirred for 10 minutes and was used to provide the anionic polyelectrolytes.

Different concentrations of zirconia solutions were prepared. The calculations of these concentrations can be found in appendix A. Before mixing ZrO_2 solution with the deionized water, both pH's were adjusted by adding HCl. The final ZrO_2 solution was used as the cationic polyelectrolytes.

4.2.2.3. Constructions of a Multilayer System

Deposition of all monolayers on the substrates was accomplished using the ISAM technique. Prior to the construction of the multilayered coating systems, several bilayers of PAH/PS119 were deposited on the substrate to promote the adhesion between the surface and the first monolayer of ZrO_2 film. Since the substrates were pre-treated as negatively charged surfaces, quartz and silicon wafers were first immersed in the PAH solution for 3 minutes. Following the immersion, the substrates were rinsed with deionized water and then immersed in the PS119 solution for another 3 minutes. The

substrates were rinsed with deionized water again. After depositing four bilayers of PAH/PS119 on the surface of the substrates with the uppermost layer of PS119, subsequent assembly of alternating ZrO_2 and polymer particles can be proceeded.

Zirconia/polymer nanocomposite thin-film coatings were deposited in the same manner as the PAH/PS119 multilayers. Water was used to rinse the substrate after each immersion. The immersion time for each solution was 5 minutes. The process of repeating cycles of ZrO_2 and polymer deposition is shown in Figure 4.3. More than 150 bilayers of ZrO_2 and PSS films were deposited on the Si (100) substrates and 10 bilayers were deposited on the quartz substrates.

4.3. Characterizations of ZrO_2 Thin-Film Coatings

4.3.1. Particle Size Distributions

Particle size distributions were measured using Malvern Zetasizer – DTS5300. The sample was dispersed in a solvent to form a colloidal system. Individual particles in a colloidal system move randomly. Their directions of motion change continuously as a result of collisions with other particles, with the suspending medium, and with the wall of the container [26]. Particle size distributions were measured by means of a change in the light intensity passing through the colloidal system. Larger particles move more slowly than smaller particles, therefore, the rate of fluctuation of the light scattered from the larger particles is slower. Photon correlation spectroscopy is used in this instrument to detect the rate of change of these light fluctuations, in turn determining the size distribution of the particles that are scattering the light.

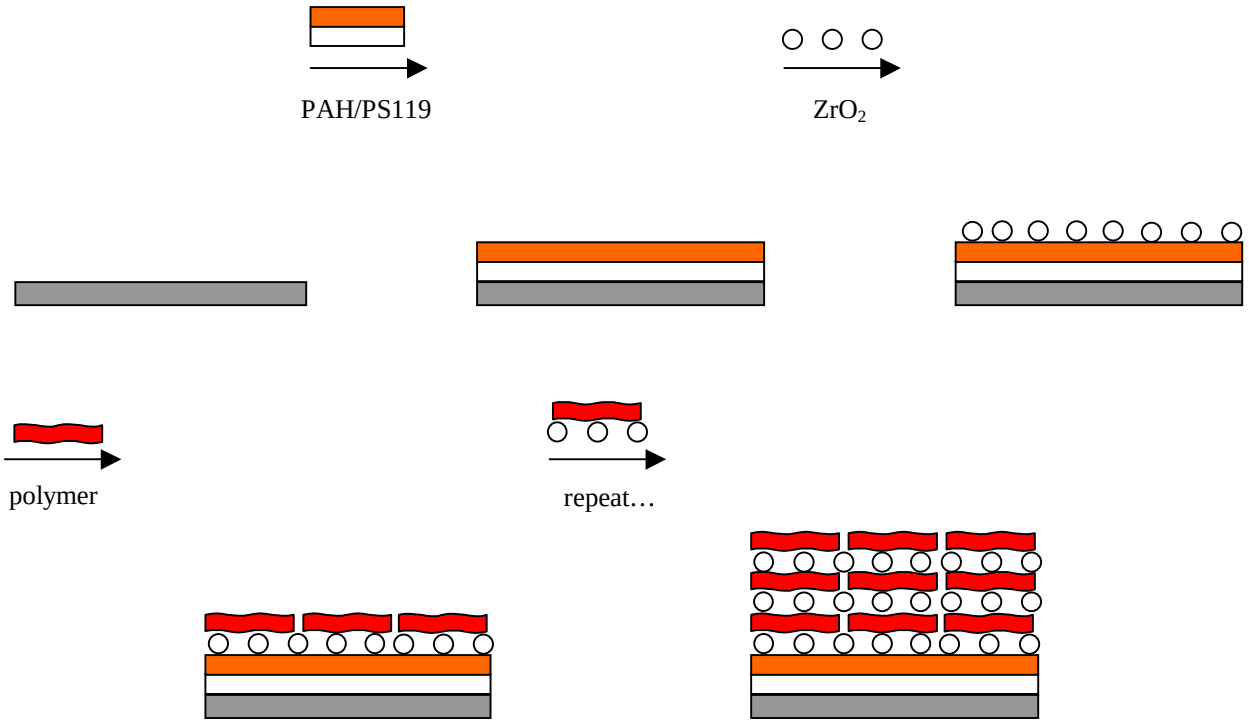

Figure 4.3. Schematic representation of multilayer fabrication of ZrO_2/polymer nanocomposite thin-film coatings.

4.3.2. Scanning Electron Microscopy and Atomic Force Microscopy

Scanning Electron Microscopy (SEM) and Atomic Force Microscopy (AFM) were used to view the surface topography of the ZrO_2 thin-film coatings. SEM generates a visualization of the surface topography utilizing a beam of accelerated electrons. The interactions between the electrons and the specimen at each point of a scan line result in electrons being given off (secondary electrons) or reflected (backscattering) which later are transferred and processed to form the representation of the surface texture. The SEM micrographs in this study were obtained using an Amray instrument. The samples were mounted on an aluminum stub without further coating. A very small amount of silver paint was applied at the surface between the sample and the aluminum stub to dissipate any excess of electrical charges.

More detailed surface images were obtained by using the AFM. Techniques of non-contact TappingMode™ and phase imaging were simultaneously utilized throughout the study. In the non-contact TappingMode™, the probe tip is excited into a resonance oscillation (sinusoidal) with a piezoelectric crystal [27]. The change in the oscillation amplitude identifies and measures the surface features, which describe the variation in surface elevation. The phase imaging technique can only analyze the planar topography of the surface. This mode recognizes the edges of structures, but is not affected by large-scale height differences. Combinations of both modes result in a more detailed surface imaging characterization.

4.3.3. Ellipsometry

An ellipsometer measures a thickness by means of changes in the state of polarization of collimated beams of monochromatic polarized light caused by reflection from the substrate surface. The ellipsometric measurements of ZrO_2 thin-film layers were completed using a Rudolph Auto-EL instrument. The analysis was always calibrated using a standard silicon wafer with SiO_2 thickness of 1097 ± 0.003 Å. The angle of incident light was fixed at 70°. The wavelength of the light was 6328 nm. The polarizer and analyzer modules were fixed at angles of 70° and 90°, respectively. The reported values in the present study were the average of three thickness measurements at the same point on the samples.

4.3.4. UV/Vis Spectroscopy

UV/Vis spectroscopy allows the measurement of the wavelength and intensity of optical absorption of near-ultraviolet and visible light by a sample. In this study, UV/Vis spectroscopy was used as a quantitative measurement to investigate the reproducibility of the ISAM technique and to correlate the thickness measurements obtained by ellipsometry. The optical absorption of multilayer assemblies were measured by a Hitachi Model U-2010 UV/Vis spectrophotometer. The range of scanned wavelengths was 200 to 630 nm. The reported values were the average of three measurements at different locations on the samples. Plots of optical absorbance versus the number of layers provide useful information about the quality and the reproducibility of the multilayer deposition process.

4.3.5. Adhesion Test

Adhesion tests were developed to study the durability of coatings and to observe stress failures. The simplest and most commonly used adhesion test is based on the use of self-adhesive tape, which is called the Scotch-tape or tape test. Prior to testing, the coating and the substrate should be cleaned and dried. The testing apparatus is shown in Figure 4.4. The test procedure is performed by pressing a specified pressure sensitive adhesive tape onto a coated surface, and then quickly peeling off the tape at an angle normal to the surface. If no material is removed from the surface, then the coating passes the test. If some of the coating is removed, then the coating is unstable and the test is inherently destructive due to material removal by the tape.

In this study, because the coatings were transparent, the assistance of UV/Vis spectroscopy measurements was used to observe any changes in the optical absorbance as a result of particle removal. AFM was also used to investigate changes in the surface structure of the film.

4.3.6. Abrasion Test

The abrasion tests were designed to evaluate and quantify the durability of the coating to any scratching, rubbing, or friction activities. There are two tests commonly used for these purposes: the cheesecloth (moderate abrasion) test and the eraser (severe abrasion) test. Both tests require clean substrate surfaces.

For the purpose of this study, only the moderate abrasion test was employed considering the low number of monolayers that were deposited on the substrate. The

Figure 4.4. Adhesion and abrasion testing apparatus.

equipment used in this test is shown in Figure 4.4. In the moderate abrasion test, a pad of cheesecloth, approximately 9.5 mm ($^3/_8$″) in diameter and 6.4 mm ($^1/_4$″) thick, is pressed against the coated surface with a force of 1.0 lbf (4.4 Newton). The cheesecloth pad is rubbed against the coated surface from one point to another over the same path for 25 complete cycles (strokes). Following the test, observations could be performed visually to investigate any deterioration of the coatings. However, if visual observation reveals no changes, a clarification may be performed using UV/Vis spectroscopy, in a similar way as that performed in the adhesion test.

4.3.7. Microhardness Measurement

Microhardness testing was used to determine the hardness of the material on a microscopic level. The measurements were performed by Micro Photonics Inc. at the Centre Suisse d'Electrnonique et de Microtechnique. A Nano-Hardness Tester (NHT) was utilized for the measurements in this study. An indenter tip with a known geometry was driven into a specific site of the material to be tested by applying an increasing normal load. When reaching a preset maximum value, the normal load is reduced until partial or complete relaxation occurs. This procedure was then repeated.

For each loading /unloading cycle, the applied load value was plotted with respect to the corresponding position of the indenter. The resulting load/displacement curves provided data specific to the mechanical nature of the material under examination. Established models were used to calculate quantitative hardness values for such data.

4.4. Results and Discussions

4.4.1. Study of the ISAM Deposition Process of Multilayer Structure

The ISAM technique has been proposed as a very promising method for fabrication of highly ordered and oriented multilayered films with detailed control of the properties of the materials at the microscopic scale. The present study demonstrated the fabrication of ZrO_2/polymer nanocomposite multilayered thin-film coatings by employing this fabrication technique. Following the deposition of PAH/PS119 layers, the procedures, as shown in Figure 4.3, started with the immersion of a modified negatively-charged substrate into a solution containing cationic polyelectrolytes. This process reversed the surface charge to be positive. The substrate was then rinsed with ultrapure water to remove any excess charged particles. Subsequently, the substrate was immersed for a second time in a solution containing anionic polyelectrolytes. After the immersion, the substrate was rinsed with the ultrapure water. This second immersion restored the initial surface charge, which was negative. Multilayer buildup was constructed based on the attraction of opposite charges of particles. Therefore, by repeating the above procedure in an alternating fashion, multilayer assemblies of ZrO_2/polymer thin-films were fabricated on the substrates.

The deposition of these multilayer assemblies was monitored by UV/Vis spectroscopy. Figure 4.5 displays the optical absorption spectra of all the polyelectrolyte solutions in water. Peaks of optical absorption bands were observed at 230, 310, and 470 nm for the PS119 solution in water and at 260 nm for the PSS solution in water. No peak was observed in the absorption spectra of the PAH and ZrO_2 solutions, however, their optical absorption intensities increased strongly as the wavelength was approaching the

ultraviolet range. Also displayed in this figure is the optical absorption spectrum of ZrO_2/polymer multilayer assemblies. Three absorption bands were observed at 225 nm, 310 nm, and 485 nm in this spectrum. These resulting peaks from the multilayer assemblies were combinations of the individual polyelectrolyte peaks. The peaks at 310 and 485 were from the optical absorption by PS119. The peak shift from 470 nm in the PS119 solution to 485 nm in the multilayered films was a result of the molecular interactions between the monolayers in the PAH/PS119 layers.

Figure 4.6 shows the optical absorption spectrum per bilayer for the ZrO_2/polymer films. As the number of bilayers increases, the optical absorption of the films also increases. No shift was observed in the maximum absorption peaks which means that no molecular aggregation occurred between the adjacent layers [22]. The Beer-Lambert law states that the change in the light intensity when it passes through a material is a function of the length it travels and proportional to the number of molecules in the material. As the number of bilayer increases, more molecules remain on the substrate which also increases the distance traveled by light. Therefore, the optical absorption intensity of the multilayered films in this study increased as the number of deposited bilayers increased.

The consistency of the deposition process is indicated in Figure 4.7 which shows a linear dependence of optical absorption with an increasing number of bilayers at 225 nm. The linear behavior of the optical absorption on this structure indicates a formation of homogeneous films. The absorption data for successive bilayers were fitted with a linear least-square regression analysis. The calculated average optical density was 0.016606 ± 0.002187 per bilayer at 225 nm. The linear nature of this deposition indicates that each layer contributes an equal amount of material to the multilayer films.

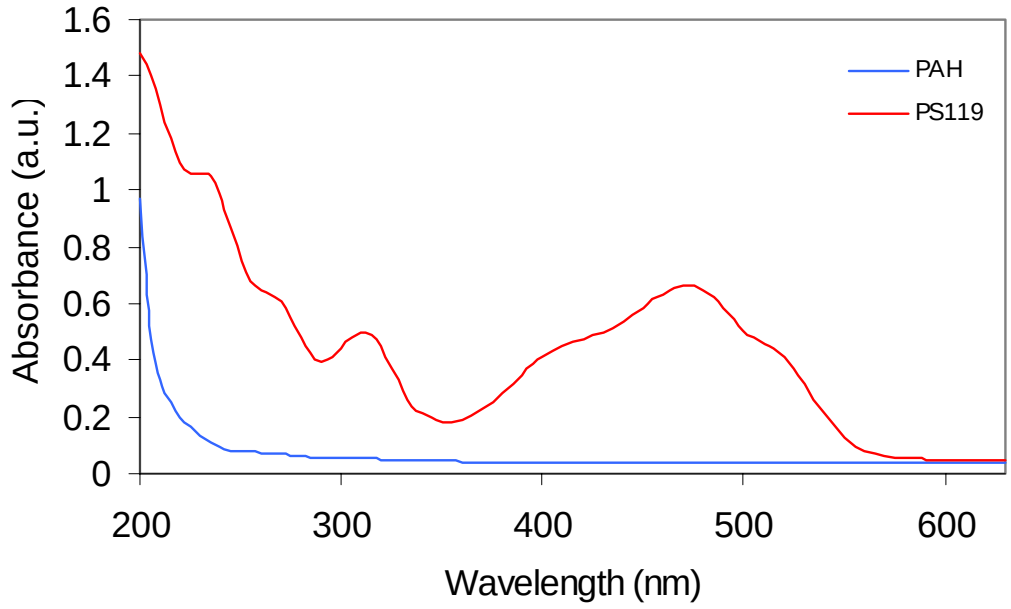

a

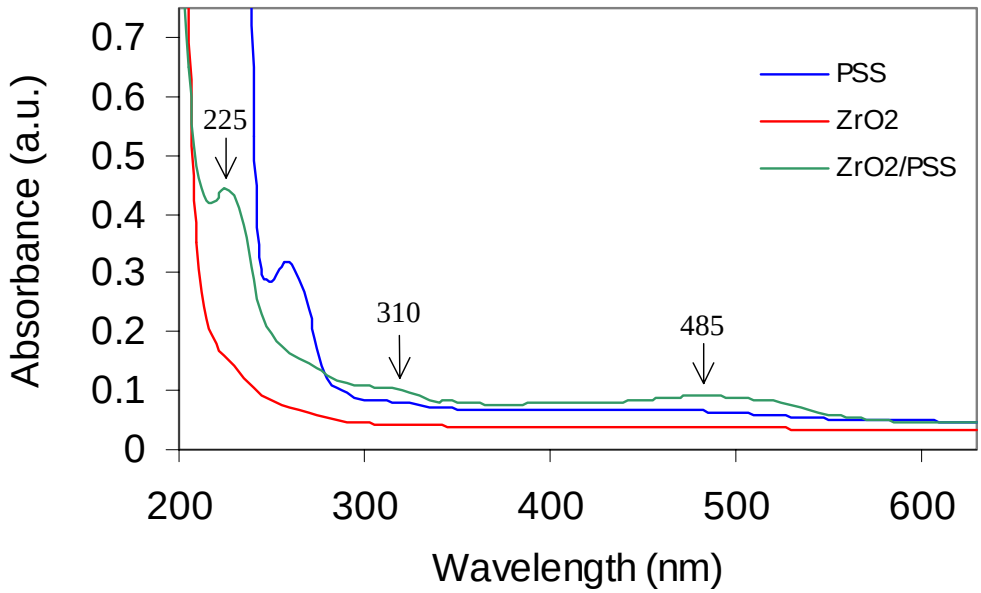

b

Figure 4.5. UV/Vis spectra of PAH, PS119, ZrO_2, and PSS solutions in water. Also shown in b is the UV/Vis spectrum of ZrO_2/PSS films deposited on a quartz substrate.

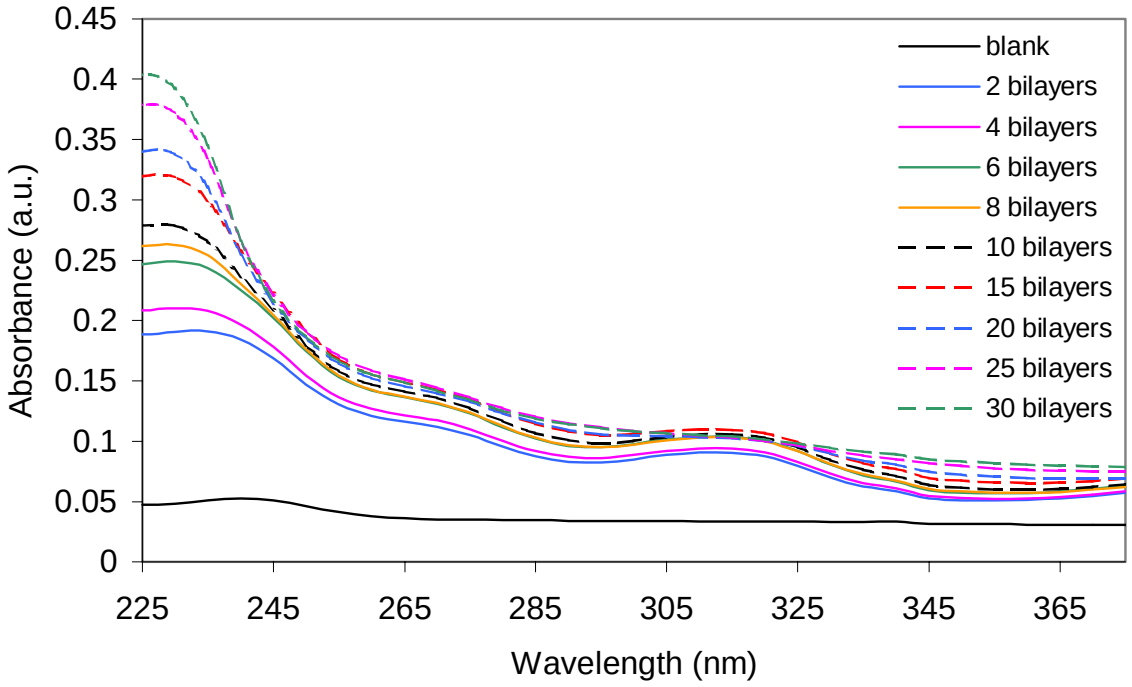

Figure 4.6. UV/Vis Spectrum of ZrO_2/PSS multilayer structure showing an increasing number of bilayers.

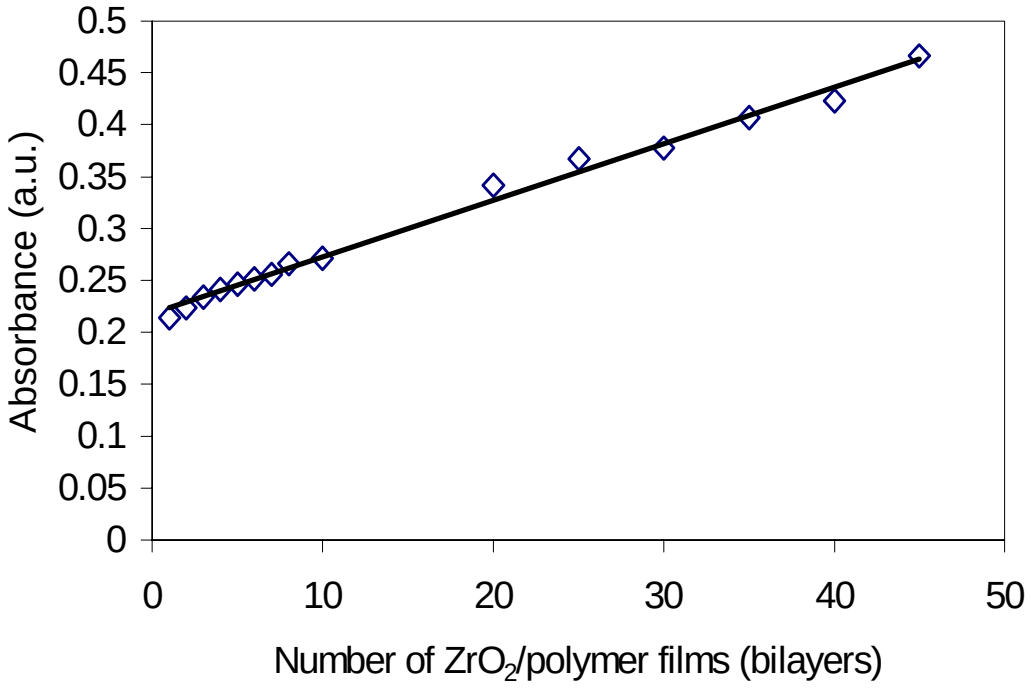

Figure 4.7. Dependence of optical absorbance of the ZrO_2/polymer multilayer film on the number of deposited bilayers (at 225 nm).

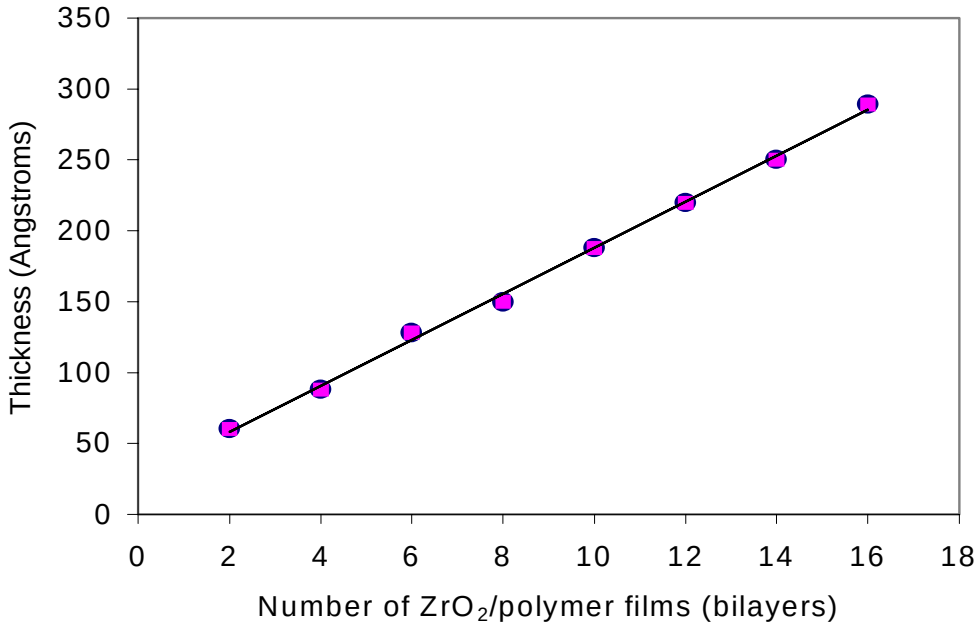

Figure 4.8. Dependence of ellipsometric thickness of ZrO_2/polymer multilayer films on the number of deposited bilayers.

The consistency of this process was also monitored by ellipsometry. The thickness was measured for every bilayer of nanocomposite film deposited on a single crystal Si (100) substrate. The concentration of the adsorbed ZrO_2 solution was 10 mg/ml. A total of 16 bilayers of ZrO_2/polymer films was deposited on the substrate. Figure 4.8 displays the stepwise development of multilayer buildup from the ellipsometry measurements. The total thickness of the multilayer was 289 Å. The thickness of each monolayer was calculated to be approximately 1.8 nm.

Both Figures 4.7 and 4.8 confirm a linear relation between the thickness and the number of layers. This indicates that each adsorbed layer contributes an equal amount of material to the multilayered structure. Therefore, highly ordered and uniform films could be fabricated on a substrate by the ISAM technique.

4.4.2. Study of Microscopic Structures of ZrO_2/Polymer Nanocomposite Films Produced by the ISAM Method

Surface imaging techniques of ZrO_2/polymer films yield information about uniformity, grain distributions, and defect formation on the surface. The microscopy study in this experiment was performed using SEM and AFM. Observations were carried out on films that were deposited on Si (100) wafers. SEM micrographs, shown in Figure 4.9, display the planar surface images of ZrO_2/polymer thin-film coatings. 200 bilayers of ZrO_2/polymer thin-films were deposited on the substrate. All micrographs in Figure 4.9 show the uniformity of film deposition on the samples. No surface damages or defects were observed during the analysis at this scale.

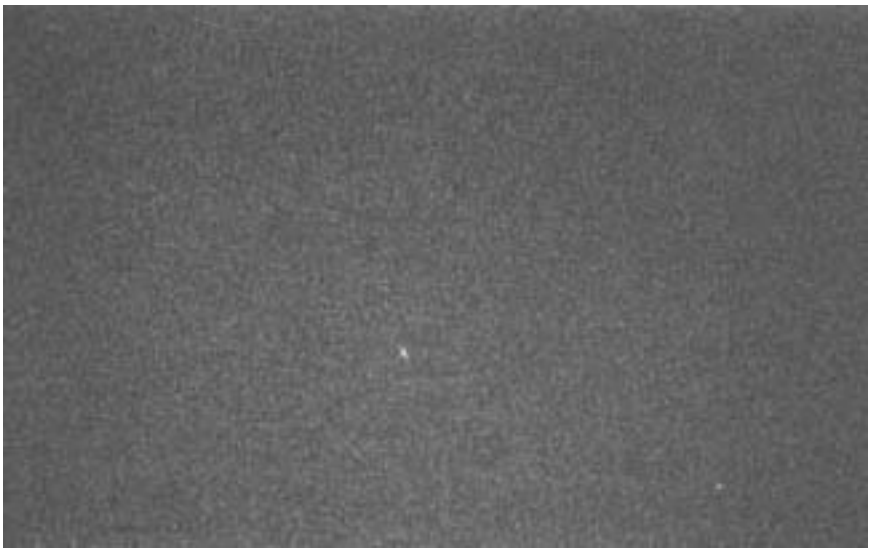

After heat treatment at 400°C for 2 hours

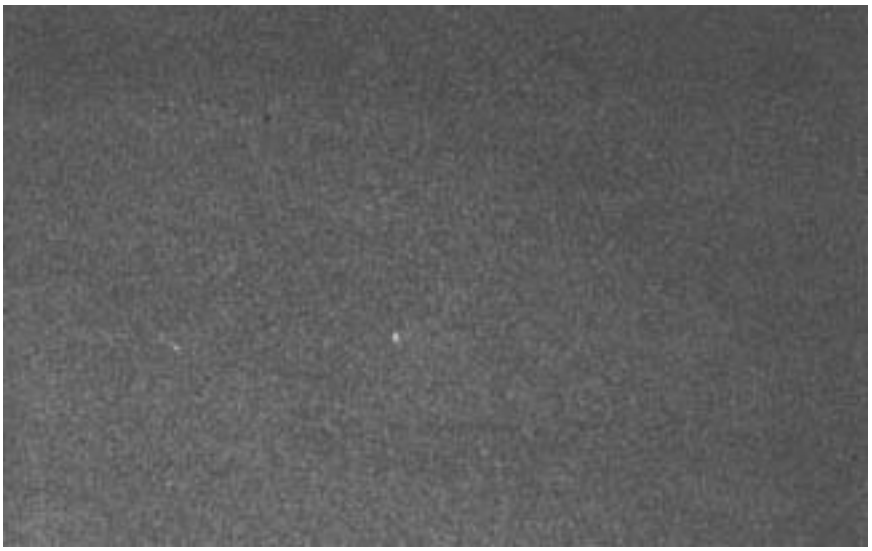

After heat treatment at 900°C for 1 hour

Figure 4.9. SEM micrographs showing the surface uniformity of ZrO_2/polymer multilayer films; ZrO_2 = 10 mg/ml.

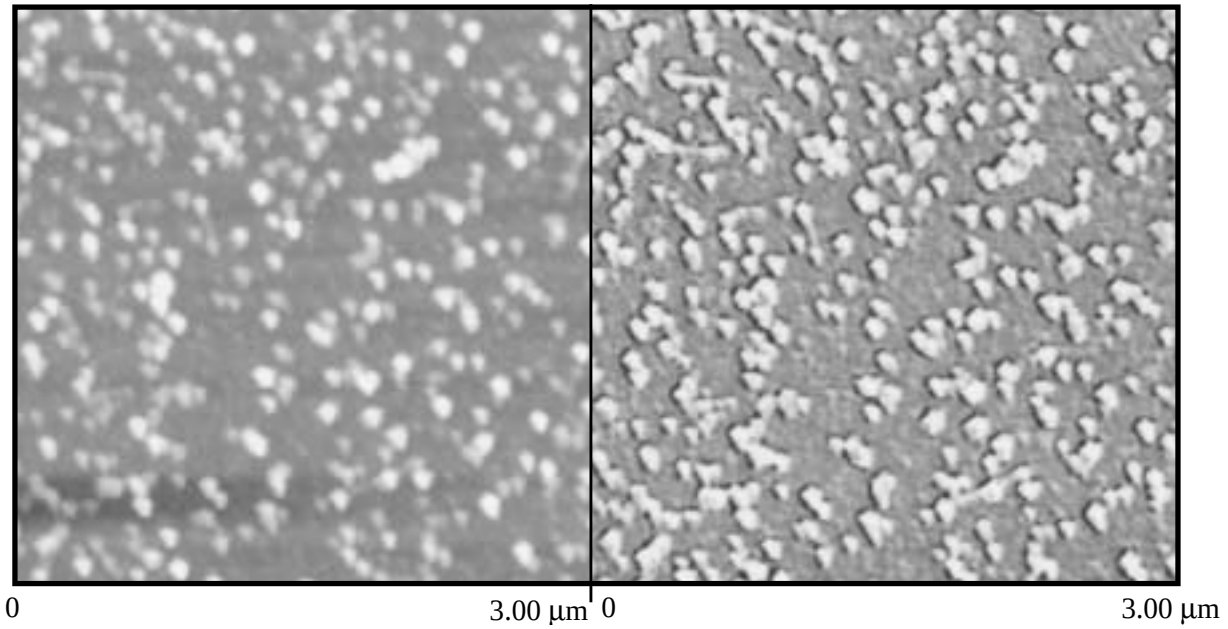

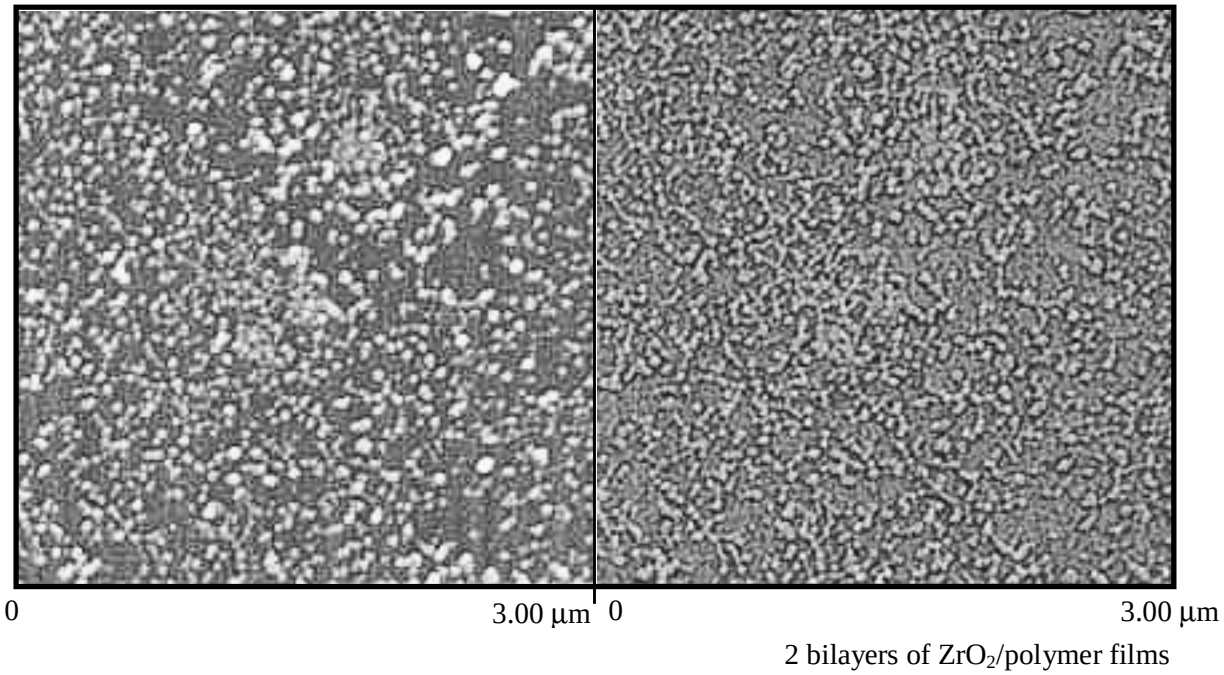

Figure 4.10. AFM images of one and two bilayers of ZrO_2/polymer films showing the closely packed layers of particles.

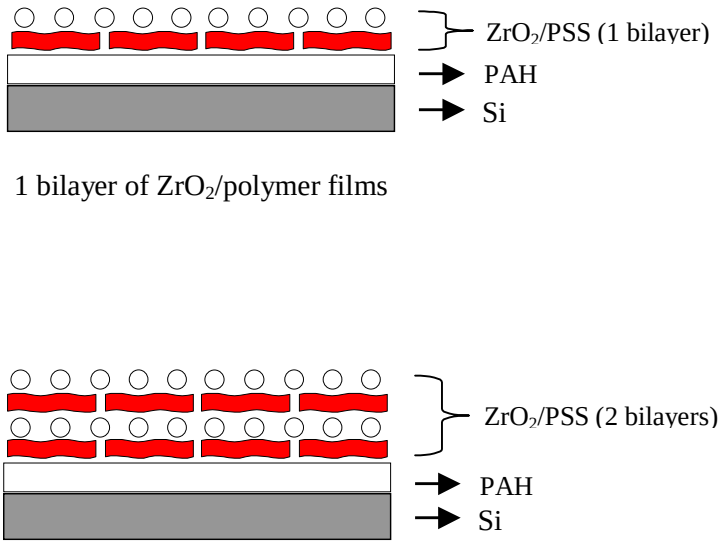

Figure 4.11. Layer structures of samples for the AFM images in Figure 4.10.

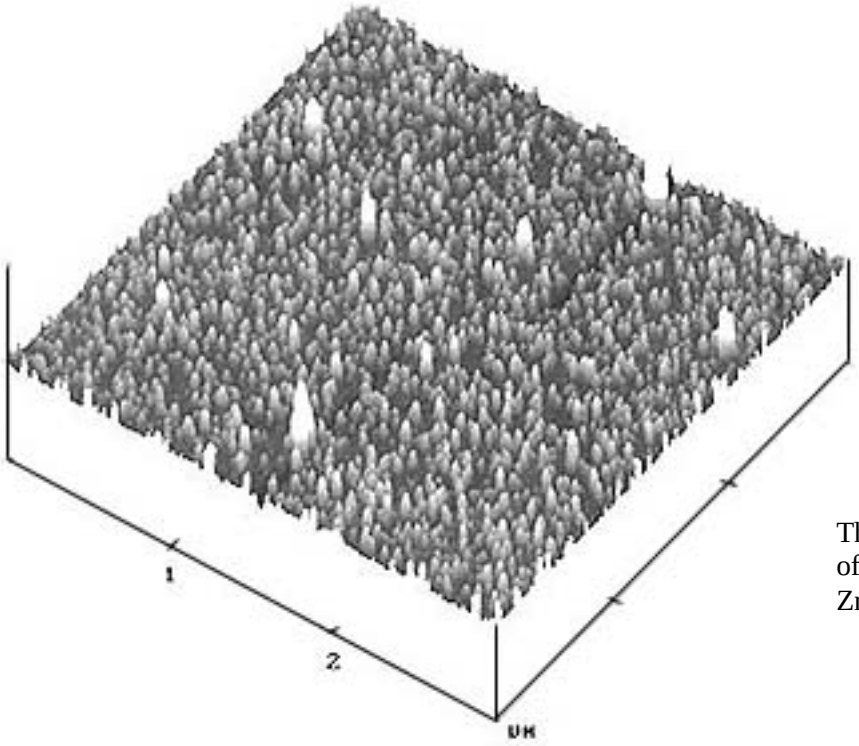

Three-dimensional image of 1 bilayer of ZrO_2/polymer films

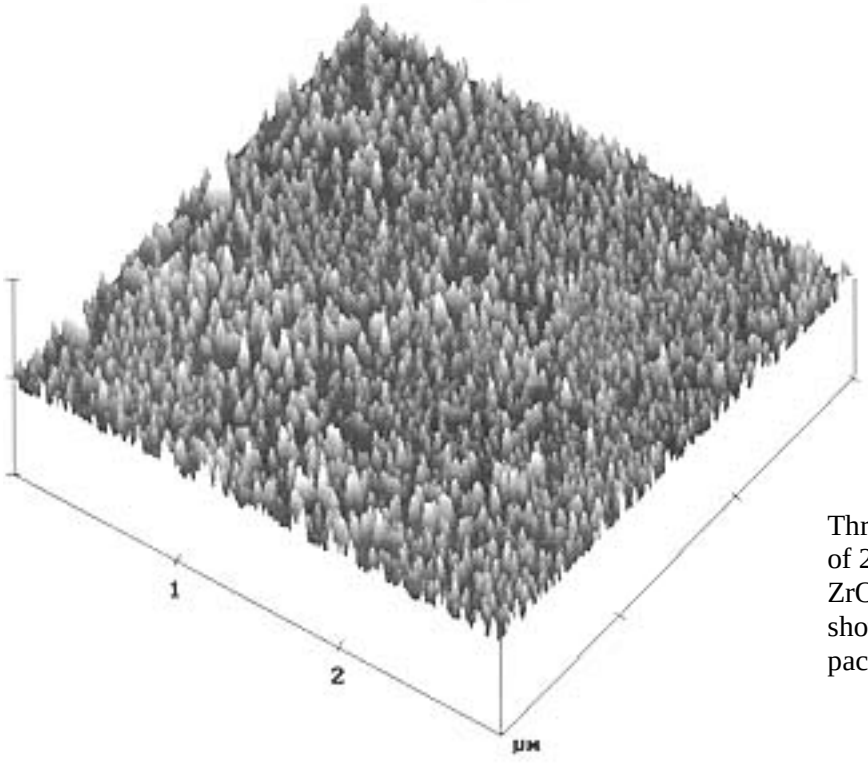

Three-dimensional image of 2 bilayers of ZrO_2/polymer films, showing more closely packed layers of particles

Figure 4.12. Three-dimensional images from AFM showing an increase in particle density on the film structures.

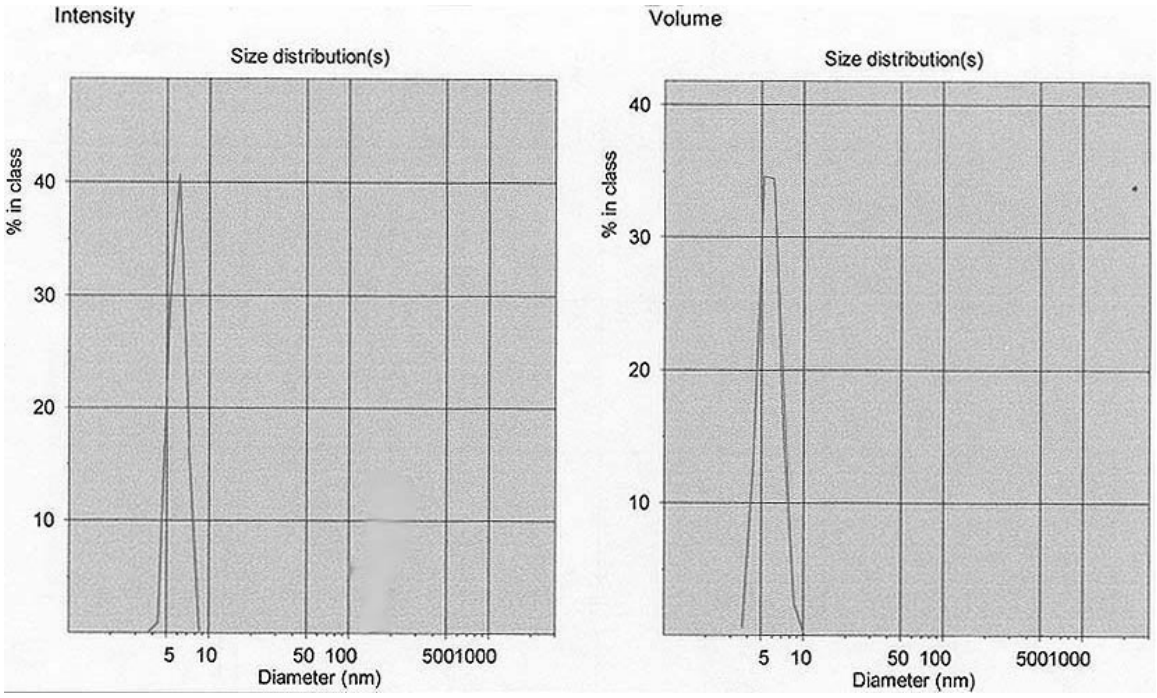

Figure 4.13. Particle size distributions of ZrO_2 colloidal system.

Further study of the structure of the films was performed by AFM. Figure 4.10 shows the planar surface images for one and two bilayers of deposited films. The left micrograph is the height image and the right micrograph is the phase image. The height image in Figure 4.10 suggests that there are different layers of films on the substrate surface. The brighter particles represent the film on the top and the darker particles represent the film underneath. The layer structure is shown in Figure 4.11. As the number of bilayers increases, the structure becomes more condensed due to an increase in the number of particles that reside on the substrate, as shown in Figure 4.12. The three-dimensional image in this figure indicates a substantially uniform dispersion of the particles.

Figure 4.13 shows the result of the particle size distribution measured by dispersing the ZrO_2 colloid in acidic water. The average particle diameters obtained from the ZrO_2 colloidal system ranged between 4 and 9 nm. In comparison, grain sizes illustrated in the AFM images ranged between 20 and 40 nm. The increase in the grain size is due to the cluster formation during the deposition process. In addition, it was calculated in section 4.4.1 that the thickness of each bilayer was approximately 1.8 nm. However, the average particle sizes are much larger than this thickness. The deposition of each bilayer was shown in Figure 4.3, where each layer of film was deposited exactly on the top of previous layer, forming an evenly horizontal surface. The actual schematic of the deposition process is described in Figure 4.14. In this figure, the particles of the next deposited layer will fall into the available spaces, such as those associated with voids or porosity, existing from the deposition of the previous layers. Thus, the films were not deposited in an even surface, but rather in a bumpy one.

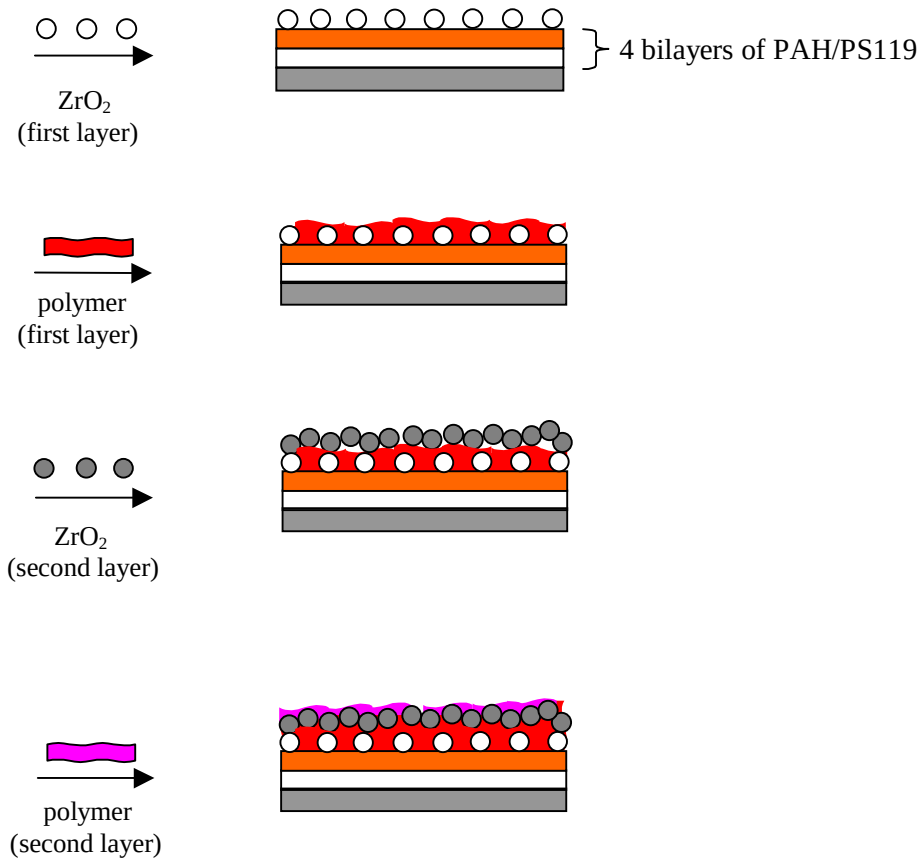

Figure 4. 14. The ISAM fabrication method of ZrO_2/polymer nanocomposites showing the formation of bumpy surfaces.

Previous studies of zirconia films prepared by other methods showed microstructural defects on the coatings. Preparation of ZrO_2 coatings by the plama spray technique requires the control of flaw size that influences the process of crack propagation in the film. Voids have also been observed to form in between grain boundarires. Electron beam evaporation produced the formation of columnar growth on the structure of such film. These undesirable defects could result in degradation of the mechanical properties of the coatings. In comparison, present study of fabrication of ZrO_2 coatings by the ISAM method has shown denser, homogeneous, and reproducible layers of films with closely defined microstructures.

4.4.3. Study of Heat Treatment of ZrO_2/Polymer Thin-Films

During heating processes, zirconia generally will undergo a phase transformation process. The change in volume associated with this transformation makes the usage of pure zirconia become difficult in many applications. Therefore, the addition of some oxides, such as CaO, MgO, Y_2O_3, into the zirconia structure to a certain degree results in a solid solution called stabilized zirconia [28]. The addition of MgO yields larger microstructures (50-100 micron), while adding Y_2O_3 yields smaller microstructures (less than 1 micron). Stabilized zirconia finds more applications due to its increased hardness, denser structure, and high thermal shock resistivity.

A heat treatment study was performed on the films deposited on Si (100) wafers. The samples were heated to two different temperatures in air for different periods of time. Different concentrations of zirconia solutions, 10 mg/ml and 40 mg/ml, were deposited

on the substrates for the purpose of this study. SEM and AFM micrographs were analyzed to investigate any structural changes on the deposited film layers. The SEM micrographs, shown in Figure 4.9, could only exhibit the uniformity of the film indicating no defect formation. However, a careful examination would result in the observation of the emerging of more defined grains.

During the heat treatment process, ceramics generally undergo several processing stages of removal of porosity, formation of new grains, and grain growth. At the same time, the system will experience a volume shrinkage as the porosity is eliminated from the structure. Further heat treatment at high temperatures could result in the changing of material properties. The ZrO_2 films in this study displayed some of these processing effects when heated.

Very distinct changes in the grain structures were observed on the AFM images as a result of different heating temperatures, however, no sign of grain growth was observed. The AFM images in Figure 4.10 of the as-deposited sample of ZrO_2 films show the grain distributions coated with the polymers. Heat treatment of the sample at 400°C for 2 hours resulted in the removal of some polymers from the structures. AFM images in Figure 4.15 illustrate that zirconia nanoparticles started to emerge on the surface. The evaporation of polymers from the films reduced the volume density of the structure. Nonetheless, zirconia nanoparticles rearranged themselves forming connections between the adjacent particles. This process eliminated voids that were formed in between grain boundaries. The void elimination process resulted in an increase in packing density of the structure.

Heat treatment at higher temperatures would accelarate the evaporation of polymers and, at the same time, promote the atomic diffusion of zirconia nanoparticles to the grain boundaries and surfaces. When the sample was heated at 900°C for 1 hour, all of the polymer in the films is evaporated. At the same time, the atomic diffusion of zirconia nanoparticles increases the fraction of particles that remain near the grain boundaries, thus increasing the density of atoms on grain boundaries. The AFM images in Figure 4.16 display the surface of ZrO_2 films after heat treatment at 900°C. It is shown that grain boundaries are very well defined, however, no grain growth was observed.

It appears that the zirconia nanoparticles in the ISAM multilayer structure might require higher temperatures than 900°C to start the grain growth process. The presence of the polymers in the film structure supressed the growth of zirconia particles. Because the film structure was very dense, higher temperatures were required to remove all polymer particles from the films.

4.4.4. Study of Varying ZrO_2 Concentrations

Previous studies, performed by Decher et al., introduced a method of tuning the average thickness of oppositely charged layers [4]. They reported that by changing the ionic strength of the polyelectrolytes by means of adding NaCl to the solution, the total film thickness could be controlled. The present study employed this method to control thickness in the ZrO_2 films by changing the concentrations of ZrO_2 solutions. Different ZrO_2 solutions of concentrations 10 mg/ml, 30 mg/ml, and 40 mg/ml were prepared. The

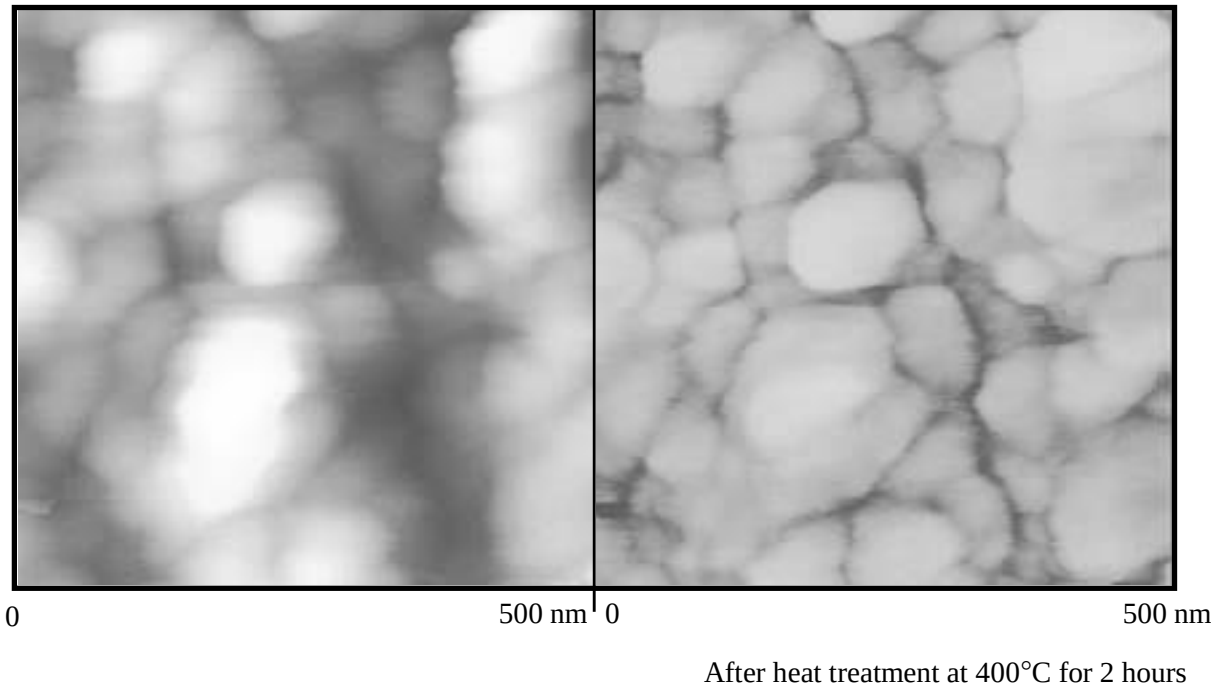

Figure 4.15. AFM images of ZrO_2/polymer coating surface. The structure consists of 150 bilayers of films; ZrO_2 = 40 mg/ml.

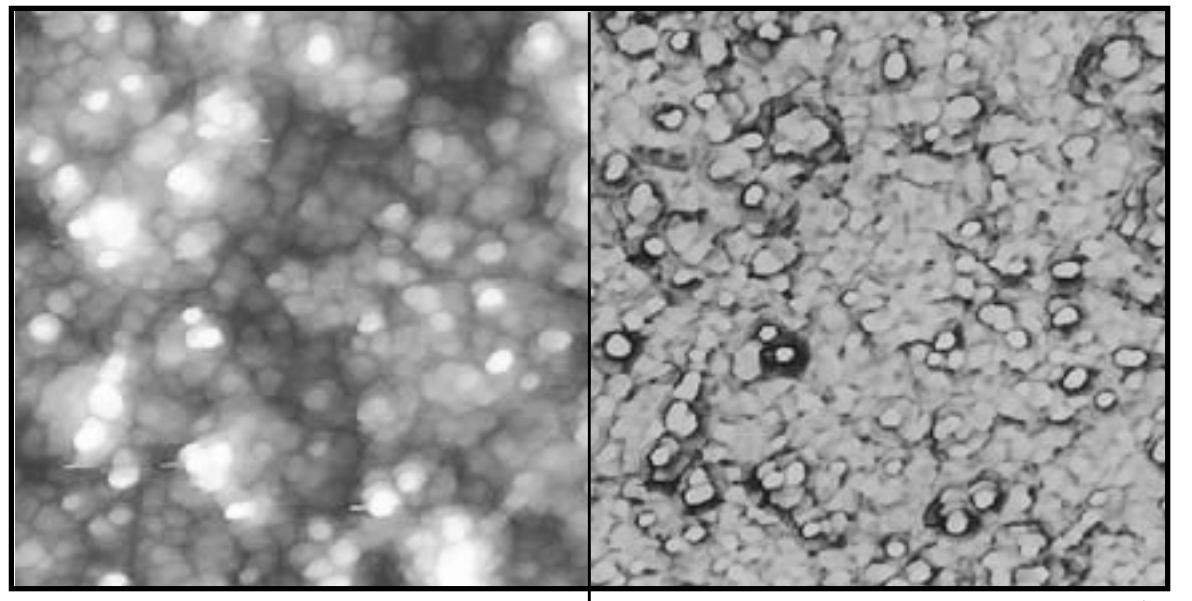

Figure 4.16. AFM images of ZrO_2/polymer coating surface. The structure consists of 200 bilayers of films; ZrO_2 = 10 mg/ml.

adsorptions of these solutions were done on three quartz substrates following the same procedures described in section 4.2.2.3. The total number of bilayers deposited was 15. The results of the UV/Vis spectroscopy measurements are shown in Figure 4.17.

It was found that increasing the ZrO_2 concentration resulted in increasing the optical absorbance. This phenomenon could explained by particle coagulation caused by the presence of excess charged ions that add to the layer thickness. Increasing ZrO_2 concentration increases the amount of oxygen ions. Since the substrate is negatively charged, the excess oxygen ions which also carry negative charges will act as counter ions for the zirconium ions. The electrostatic attractions between the zirconium and oxygen ions will appear stronger than that between the zirconium ions and the substrate. In addition, there are also some electrostatic repulsions between the substrate and the oxygen ions. Therefore, the atoms of zirconium and oxygen would cluster together producing a thicker layer of film resulting in an increase in optical absorbance.

To assist in characterizing the effect of salt concentrations on the thickness film layer, ellipsometry measurements were performed on the films that were deposited on silicon substrates. Figure 4.18 shows the linear behavior of the thickness dependence on the number of deposited bilayers of two different ZrO_2 concentrations. The thickness of 12 bilayers of films containing 10 mg/ml ZrO_2 is 220 Å. In comparison, the total thickness for the same number of bilayers for films containing of 30 mg/ml ZrO_2 is 301 Å. Thus, the results showed that increasing ZrO_2 concentrations would increase the film thickness.

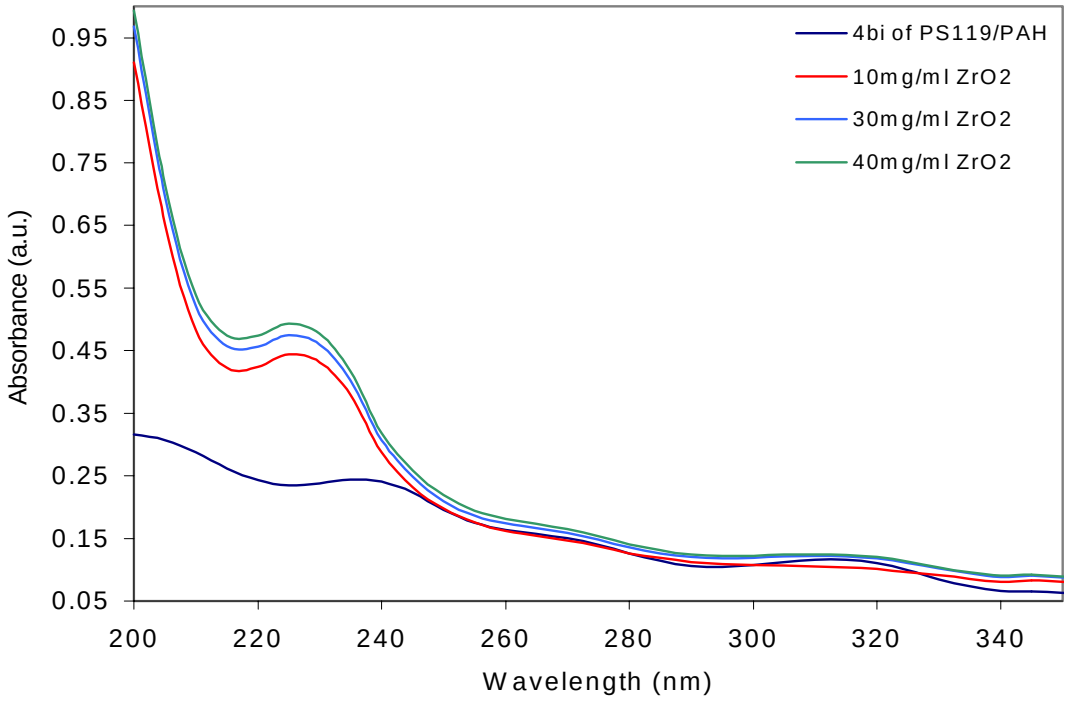

Figure 4.17. UV/Vis spectra showing increasing optical absorption for different concentrations of ZrO_2 solutions.

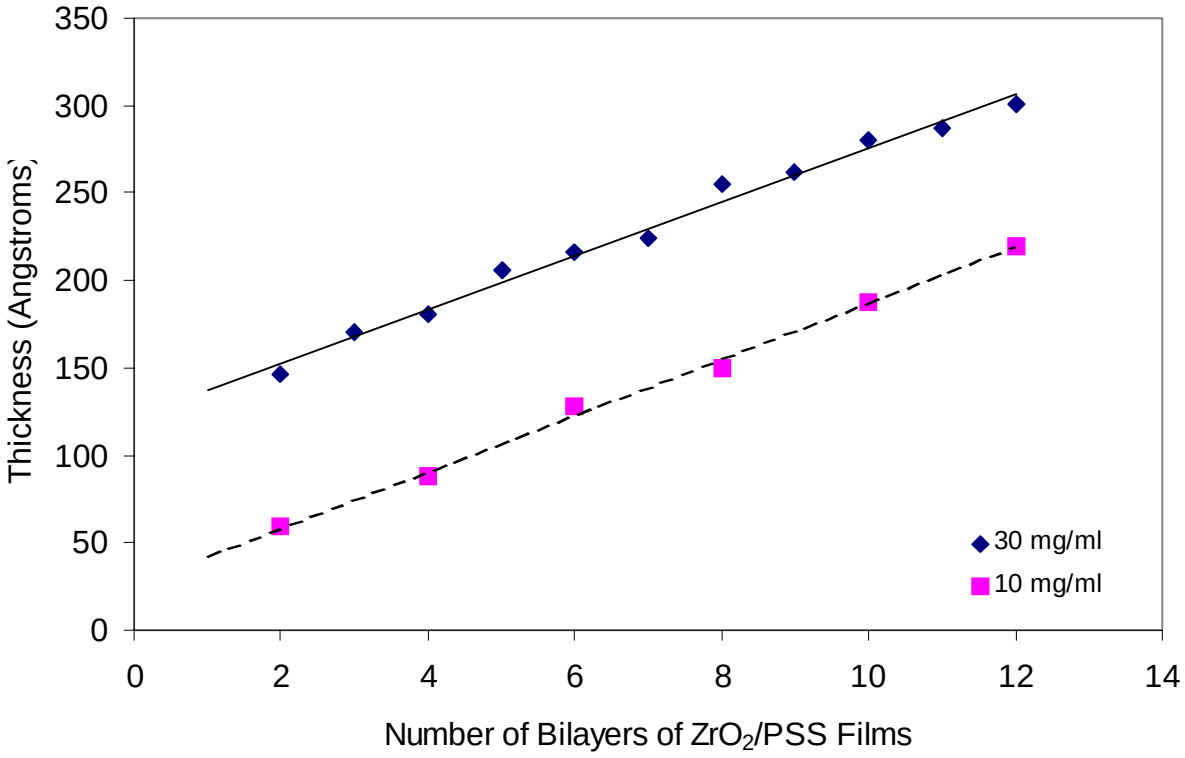

Figure 4.18. Thickness dependence of the ZrO_2 concentrations.

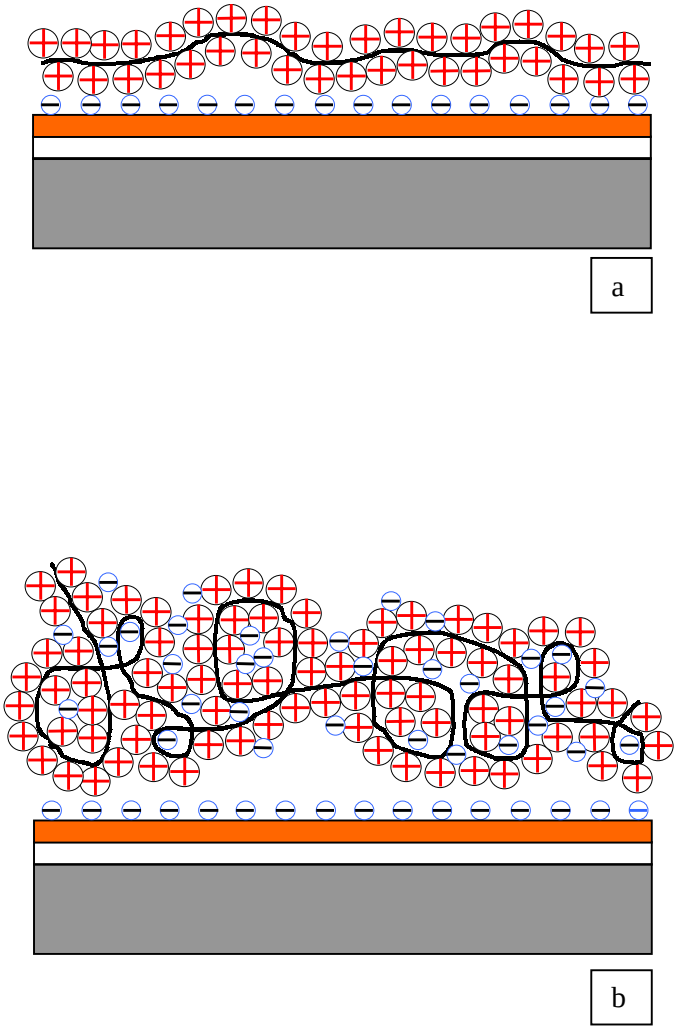

Figure 4.19. Flat (a) and loopy (b) structures of ISAM monolayer due to the presence of counter ions.

When a monolayer of ZrO_2 solution without any excess charged particles is adsorbed on a substrate, it will be deposited in a "flat" structure. The surface charge provides just enough electrostatic attraction for the zirconium ions to balance the attraction from the opposite direction by the oxygen ions. Moreover, when the substrate is immersed in a ZrO_2 solution with an increased concentration, a "loopy" structure would be deposited on a substrate because of the presence of excess charged nanoparticles. This loopy structure forms a thicker monolayer of films. The schematics of these two structures are shown in Figure 4.19.

4.4.5. Study of Changes in Some Mechanical Properties of Zirconia Thin-Film Coatings

The study of the adhesion of ZrO_2 coating layers prepared by the ISAM method was performed on a quartz sample. The concentration of ZrO_2 solutions was 10 mg/ml. The number of ZrO_2/polymer films deposited on the substrate was 15 bilayers. The test was conducted following the procedure described in section 4.3.6. The optical absorption was measured by UV/Vis spectroscopy directly after the sample was tested. The results are shown in Figure 4.20. AFM images of the surface after the adhesion test are shown in Figure 4.21.

Abrasion tests were performed on the quartz samples. The concentration of the adsorbed ZrO_2 solution was 40 mg/ml. As many as 15 bilayers of ZrO_2/polymer films were deposited on the substrate. The tests were conducted following the procedure

described in section 4.3.7. After the test, the optical absorption of the sample was measured by UV/Vis spectroscopy.

Both the adhesion and the abrasion tests resulted in removal of particles from the surface of the films. The AFM images in Figure 4.21 show distorted grain structures that follow a pattern of parallel lines on the film surface. These lines were formed due to the removal of the tape from the surface during the adhesion test. The UV/Vis spectrum demonstrated a decrease of optical absorption intensities after the tests were performed. The damaged nanoparticle structure affects the absorbance reading because of the scattering effect of the surface non-uniformity. From the Beer-Lambert law, it was shown that the absorption intensity is proportional to the amount of molecules on the samples. Rubbing of the surface during the abrasion tests removed some particles from the surface, which means that the number of molecules on the film decreased. A path of damaged film was observed visually on the ZrO_2/polymer nanocomposite films when the sample was held against a light. Therefore, UV/Vis spectroscopy should respond to some variance in the optical absorption of the film. The results of these measurements are shown in Figure 4.22.

The use of ultra microindentation instruments enables the determination of some of the mechanical properties of thin-films, such as hardness and elastic modulus. Most of the systems are able to obtain information for forces down to a sub micro-Newton levels, and displacements down to a few nanometers. The zirconia films that were deposited on silicon wafer substrates were indented using a Berkovich diamond indentor. Samples processed with different heat treatments were tested. The concentration of the ZrO_2

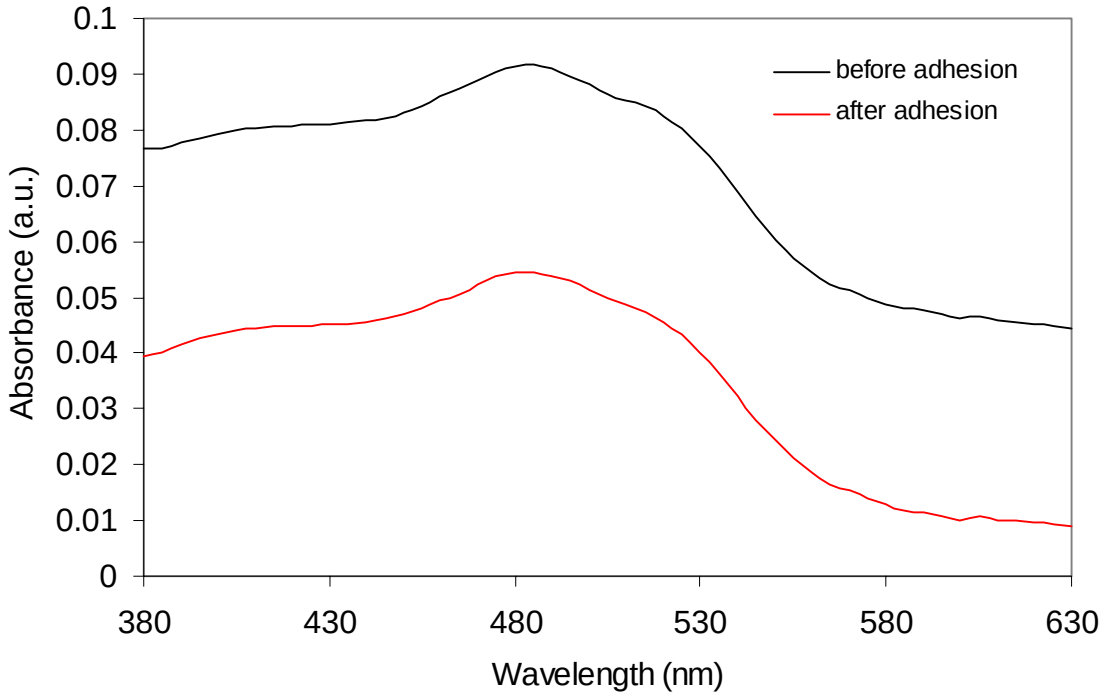

Figure 4.20. UV/Vis spectrum after the adhesion test showing a decrease of optical absorption.

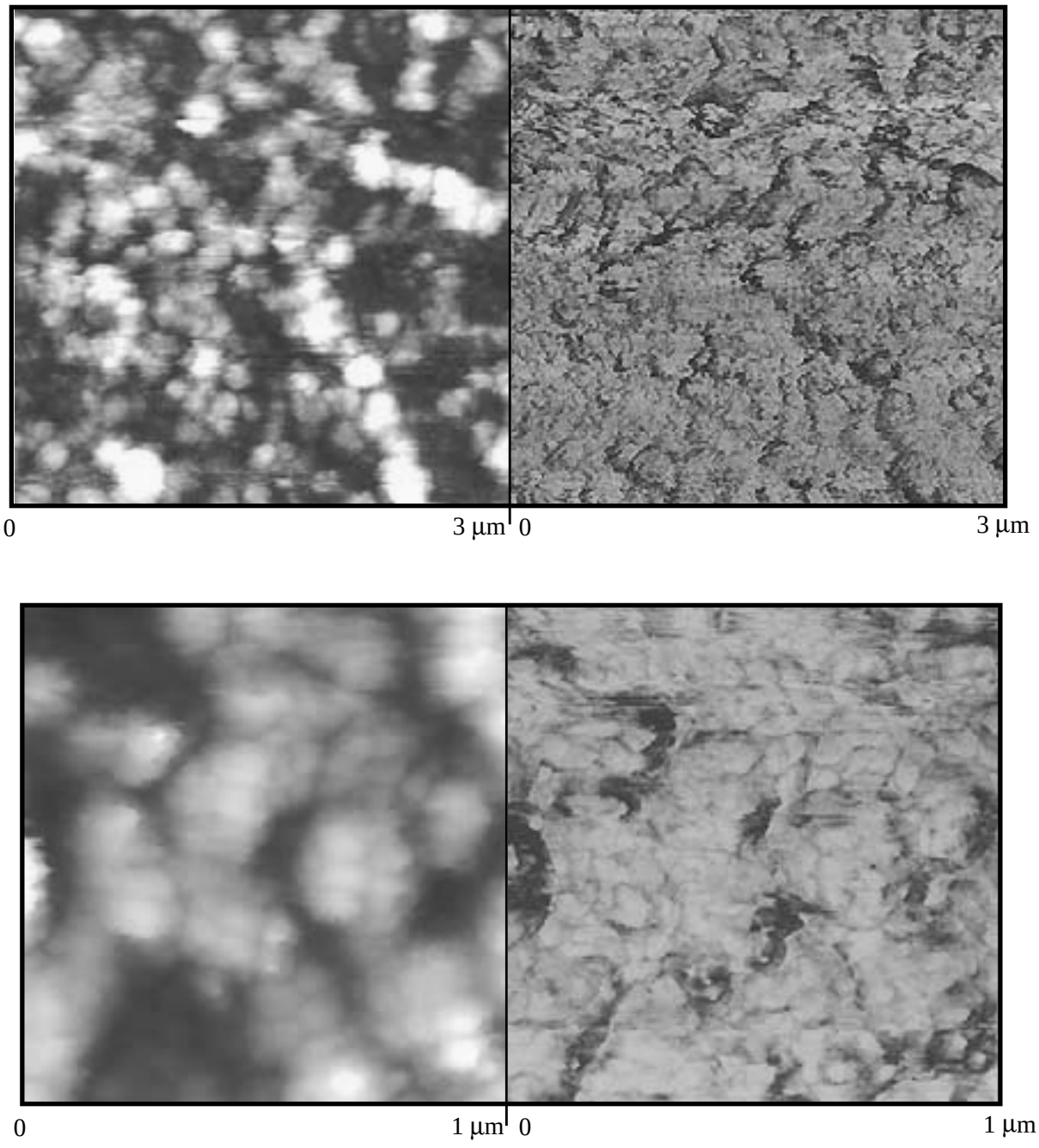

Figure 4.21. AFM images after the adhesion test showing distorted particles on the coating surface.

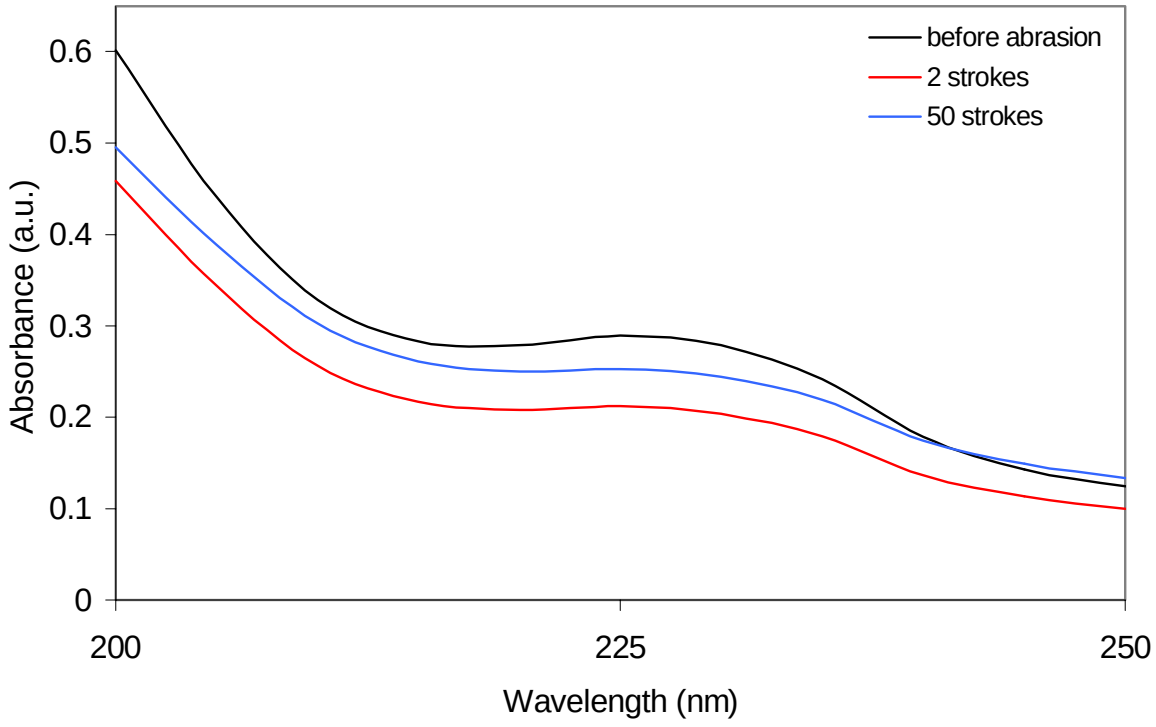

Figure 4.22. UV/Vis spectrum after the abrasion tests showing a decrease in optical absorption.

solution was 40 mg/ml. The multilayer structures consisted of 200 bilayers of ZrO_2/polymer films.

Hardness indentations were obtained by applying a force of approximately 10 mN on the sample with a maximum indentation depth of 100 nm. A series of 10 indentations was carried out on the as-deposited and 900°C treated samples, and 7 indentations on the 400°C treated sample. The reported values are the average of a series of these indentations. A typical load/displacement curve is shown in Figure 4.23. The Vickers hardness was determined from the maximum load, P_{max}, divided by the projected contact area, A_c. Notice how the area under the curve is reduced as the temperature increases, which corresponds to an increase in hardness values. The results of these measurements are listed in Table 4.1.

Vickers microhardness of ZrO_2 thin-film coatings prepared by the ISAM method (which will be referred to as the ISAM samples) demonstrated higher values in comparison to ZrO_2 coatings prepared by other methods. The microhardness values of the ISAM samples at room temperature were 2.24 GPa at an applied load of 1 mN. Earlier studies showed that sputter-deposited ZrO_2 coatings with a deposition temperature of 80°C failed the hardness measurement because of visible peeling of the film before indentation [1]. Nevertheless, this study also suggested that the deposition temperatures affected the microhardness values. As the temperature increased, the decrease in void concentration due to diffusion was much more pronounced, thus increasing the microhardness of the films. Similar behavior was observed in the Vickers hardness measurements of the ISAM samples.

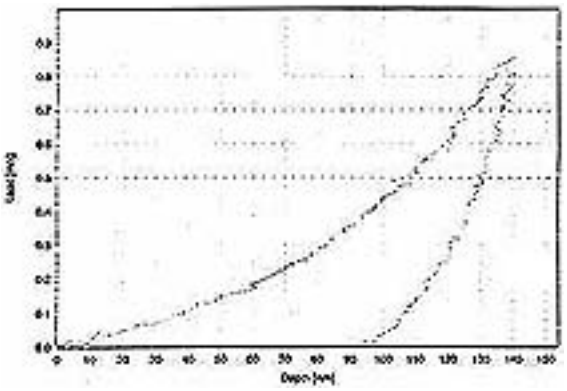

Typical load/displacement curve of as-deposited sample

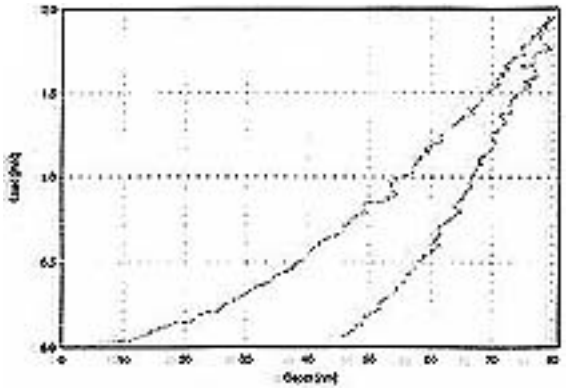

Typical load/displacement curve of sample heated at 400°C for 2 hours

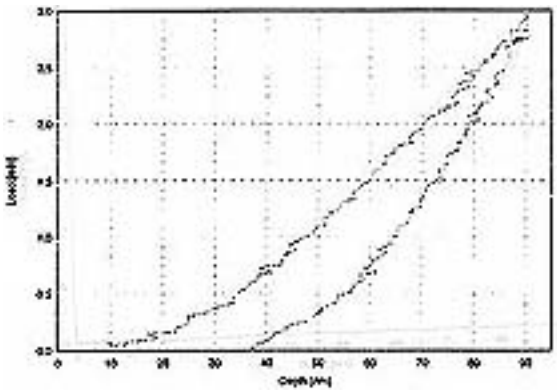

Typical load/displacement curve of sample heated at 900°C for 1 hour

Figure 4.23. Load/displacement curves of ZrO_2/polymer thin-film coatings after different heat treatments.

Table 4.1. Microhardness values of ZrO_2/polymer thin-film coatings of different heat treatments.

Sample identification	Max. Applied Force (mN)	Vickers Hardness (GPa)
As-deposited	1	2.224
	1	2.282
	1	2.211
	1	2.142
	1	2.222
	1	2.342
	1	2.406
	1	2.293
	1	2.154
	1	2.144
	Average	**2.242**
400°C – 2 hrs	2	18.179
	2	19.407
	2	19.523
	2	19.417
	2	20.219
	2	19.269
	2	19.166
	Average	**19.311**
900°C – 1 hr	3	25.569
	3	23.949
	3	27.101
	3	24.170
	3	26.154
	3	25.700
	3	24.026
	3	24.612
	3	25.009
	3	25.002
	Average	**25.129**

An increase in the hardness values with a decrease in applied load has been observed for ceramic systems. The reported microhardness values of as-thermally sprayed (at a load of 245 mN) and laser-treated stabilized zirconia coatings are 9 and 21 GPa, respectively [1]. Different studies showed a maximum microhardness value of 22.07 ± 1.47 GPa for zirconia coatings prepared by sputter deposition [1]. In the present study, a maximum coating hardness value of 25.13 GPa was observed, which was obtained from the sample that was heated to 900°C. The applied load was 3 mN, which are three orders of magnitude less than that used to evaluate the microhardness of the sputter-deposited zirconia coatings.

Higher values of Vickers microhardness of ZrO_2 coatings prepared by the ISAM method can be explained by the increase in packing density of the coating structure and surface interactions between the atoms near the grain boundaries. Fabrication of ZrO_2 thin-film coatings by the ISAM method results in the formation of a very dense and homogeneous structure. No void formation was observed, which demonstrated a structure with a high packing density. There is also a factor of strengthening mechanism by the Hall-Petch theory. The theory states that the hardness of a material increases as the grain diameter decreases. Although the high energy during the sputtering would result in the removal of atoms and impurities from the substrate surface, the average grain diameter produced in this fabrication is two orders of magnitude higher than that of the grain size of the ISAM samples. Therefore, comparisons between both Vickers microhardness test showed that the ISAM samples have higher values.

As the temperature of the heat treatment was increased, atomic diffusion of nanoparticles became more rapid. It was explained earlier that the nanoparticles would

diffuse to the grain boundaries, thus increasing the fraction of atoms that reside near the grain boundaries. More particles near the grain boundaries promote ionic attraction between the nanoparticles which also increases the hardness of the material. Therefore, by increasing the heating temperature, materials with improved hardness could be created.

Chapter 5

Conclusions and Future Work

5.1. Conclusions

The fabrication of zirconia multilayer assemblies by the ISAM technique has been shown to produce very dense, homogeneous thin-film coatings with improved properties. Highly ordered and uniform multilayered coatings can be successfully assembled by the ISAM method. The deposition of alternating oppositely charged polyelectrolytes resulted in uniform particle distributions where each layer contributed the same amount of material to the multilayered structures. The thickness of each layer was controlled by changing the number of counter ions within the structure. Understanding the ISAM method and appropriate selection of material properties would lead to fabrication of coatings of multilayer structures with tailored properties.

The presence of nanophase zirconia in the multilayered structures improved the mechanical properties of the coatings. Because of their very small-scale sizes and close packing of the particles, negligible void formation between the grain boundaries was allowed. As a result, the packing density of the structure was increased. In addition, the

close packed arrangement of the atoms caused more particles to reside near the grain boundaries, resulting in stronger surface interactions between the nanoparticles. In conjunction with an increased packing density, the surface interactions and the strong ionic attractions between the oppositely charged particles made the material harder and stronger.

The heat treatment of zirconia thin-film coatings affected the structure of the film, which in return also influenced the coating properties. As the temperatures increased, zirconia nanoparticles started to come to the surface as a result of the evaporation of the polymers. Smaller amounts of polymers in the film structure increased the microhardness values of the coatings. However, it appeared that the presence of polymers in the film structure suppressed the growth of the zirconia particles, even when the samples were heated to 900°C. Therefore, higher temperatures are required to observe any grain growth in the structures. The present study has shown that heat treatment of zirconia thin-film coatings improved the coating mechanical properties. By increasing the heating temperature, more atoms diffused to the grain boundaries and surfaces, resulting in stronger surface interactions between the adjacent particles, which increased the microhardness of the coatings.

5.2. Future Work

Further improvements in the coating properties would be a great benefit for many technology applications. Several suggestions for future studies can be drawn from the results of the present studies.

5.2.1. Study of Thermal Stability of the Zirconia Coatings Prepared by the ISAM Method

Materials for thermal barrier coating applications require good thermal insulation and thermal shock resistance characteristics. The thermal barrier coatings are subject to a maximum operating temperatures as high as 950°C. The thermal cycling during operation could produce high internal stresses due to the high temperature differences. Gradual transition in the thermal conductivity across the coating layer could reduce the internal stresses because of gradual temperature differences.

Zirconia has been used in gas turbine components because of its low thermal conductivity and high thermal expansion coefficient. Understanding the thermal behavior of zirconia coatings prepared by the ISAM method would be an advantage. Experiments of thermal stability of the zirconia coating can be outlined by planning a thermal cycle procedure where the sample would be heated up to a certain temperature and then cooled down. The procedure is repeated until the sample fails. Coatings of different thicknesses should be prepared to observe the effects of gradual transition of thermal conductivity. Such coating structures could be a great benefit for thermal barrier coating applications.

5.2.2. Study of Phase Transformation of Zirconia Coatings Prepared by the ISAM Method

Zirconia attains three different crystal structures at different temperatures, namely monoclinic, tetragonal, and cubic. In the form of cubic crystal structure, zirconia has the

highest hardness values due to the arrangements of the atoms. However, cubic zirconia is not stable at room temperature. The phase transformations of zirconia depend on its grain size and method of fabrication. The mechanical properties of zirconia could be controlled by controlling the martensitic transformation. It would be an advantage to understand the phase transformations of zirconia fabricated by the ISAM technique.

Experiments could be constructed by heating the zirconia coating to different temperatures by considering its phase diagram. Observation of any phase transformation could be performed by x-ray diffraction (XRD). Thermogravometric analysis (TGA) could be used to investigate the evaporation of the polymers from the coating structure. Following these experiments, microhardness values of the samples should be measured to observe any changes in mechanical properties.

5.2.3. Study of Nanocomposite Coatings of Zirconia and Alumina

Zirconia-alumina composite coatings have been used for thermal barrier applications. Combinations of good interfacial adhesion of alumina, the fine crystalline structure of the nanophase materials, increased hardness and the high chemical and thermal durability of zirconia would improve the performance of the coatings.

Zirconia-alumina nanocomposite coatings could be fabricated by the ISAM method. Multilayers of zirconia-alumina coatings with different structures and thicknesses are proposed to investigate the improvements in coating properties. Characterizations could be done in the same way as used in the present study with the addition of thermal stability and phase transformation studies. It could be expected that

the properties of these new nanocomposite coatings would be superior in comparison to coatings of previous studies.

References

1. M. Pakala, H. Walls, and R.Y. Lin, J. Am. Ceram. Soc., **80** [6], 1477 (1997).
2. A. Jamting, B. Ben-Nissan, I. Ashcroft, M.V. Swain, and J.M. Bell, Mat. Res. Soc. Symp. Proc., **356**, 711 (1995).

   A. Kobayashi, Surface and Coating Technology, **90**, 197 (1997).
3. M.S.J. Hashmi, J. Materials Processing Technology, **32**, 407 (1992).
4. G. Decher and J. Schmitt, Progr. Colloid Polym. Sci., **89**,160 (1992).
5. J. D. Hong, K. Lowack, J. Schmitt, and G. Decher, Progr. Colloid Polym. Sci., **93**, 98 (1993).
6. J. Schmitt and G. Decher, Advanced Materials, **9** [1], 61 (!997).
7. G. Decher, J. D. Hong, J. Schmitt, Thin Solid Films, **210/211** [1-2], 831 (1992).
8. G. M. Whitesides, J. P. Mathias, and C. T. Seto, Science, **254**, 1312 (1991).
9. R. P. Feynman, "There's Plenty of Room at the Bottom," adapted from the World Wide Web at http://nano.xerox.com/nanotech/feynman.html, Nanophase Technologies Corporation, Burr Ridge, Illinois.
10. R. W. Siegel, Nanophase Materials in Encyclopedia of Applied Physics, v. 11, G. L. Trigg (ed.), VCH, 173 (1994).
11. R.W. Siegel, Scientific American, **275** [6], 74(1996).
12. R.W. Siegel, Materials Science and Engineering, **B19**, 37 (1993).
13. R.W. Siegel, Physics Today, **46**, 64 (1993).
14. R.W. Siegel, Annu. Rev. Mater. Sci., **21**, 559 (1991).

15. R. W. Siegel, “What Is So Special About Nanostructured Materials and Coatings?” adapted from World Wide Web page at http://www.nanophase.com//FRAME/NANOINFO/Siegel2.html, Nanophase Technologies Corporation, Burr Ridge, Illinois.
16. R. Dagani, Chem. and Eng. News, **70**, 18 (1992).
17. D. R. Askeland, The Science and Engineering of Materials, 2nd ed., PWS-KENT Publishing Company, Boston, 1989.
18. R.W. Siegel, Materials Science and Engineering, **A168**, 189 (1993).
19. R.H. Tredgold, Reports in Progress Physics, **50**, 1609 (1987).
20. G.G. Roberts, Advances in Physics, **34**, 475 (1985).
21. O. N. Oliveira, Jr., Brasilian Journal of Physics, **22**, 60 (1992).
22. Yanjing Liu, “Characterization and Patterned Polymer Films from a Novel Self-Assembly Process,” Dissertation for the degree of doctor in philosophy, Virginia Polytechnic Institute and State University, 1996.
23. G.M. Whitesides, Scientific American, **273**, 146 (1995).
24. R.C. Merkle, “It’s a Small, Small, Small, Small World,” adapted from World Wide Web page at http://web.mit.edu/afs/athena/org/t/techreview/www/articles/fm97/merkle.html
25. G.W. Meetham, J. Vac. Sci. Technol. A, **3** [6], 2509 (1985).
26. At the Forefront of Particle Science, User Manual Malvern Zetasizer 1000/2000/3000, Malvern Instruments Ltd., Spring Lane South, Malvern, 1.8 (1996).
27. Adapted from World Wide Web page at http://www.di.com, Digital Instruments, Santa Barbara, California.

28. Adapted from World Wide Web page at http://www.stanfordmaterials.com/zro2.html, Stanford Materials Company, San Mateo, California.

Appendix A

Formulas and Calculations of ZrO_2 Solutions

Known: Density of the ZrO_2 colloidal solution = 1.26 gr/mL

Concentration (C)

Total volume of solution (V)

Find: Total volume of ZrO_2 solution needed (V_{ZrO_2})

Total volume of deionized water (V_{H_2O})

Calculations:

1. Find the required amount of ZrO_2 (in grams) for the desired concentration.

$$Mass(M\ in\ grams) = C \times V$$

2. Find the required volume of ZrO_2 solution based on result on 1.

$$V_{ZrO_2}(mL) = \frac{M(gr)}{1.26\,g/mL}$$

3. Find the required volume of H_2O to make the final solution of volume V.

$$V_{H_2O} = V - V_{ZrO_2}$$

Examples:

a. Known: Density of ZrO_2 = 1.26 gr/mL

C = 10 mg/mL

V = 50 mL

Calculations:

1. $M = (10\,mg/mL) \times 50\,mL = 0.5\,gr$

2. $V_{ZrO_2} = \frac{0.5\,gr}{1.26\,g/mL} = 0.40\,mL$

3. $V_{H_2O} = 50\,mL - 0.40\,mL = 49.60\,mL$

b. Known: Density of ZrO_2 = 1.26 gr/mL

C = 30 mg/mL

V = 50 mL

Calculations:

1. $M = (30\,mg/mL) \times 50\,mL = 1.5\,gr$

2. $V_{ZrO_2} = \frac{1.5\,g}{1.26\,gr/mL} = 1.19\,mL$

3. $V_{H_2O} = 50\,mL - 1.19\,mL = 48.81\,mL$

c. Known: Density of ZrO_2 = 1.26 g/mL

C = 40 mg/mL

V = 50 mL

Calculations:

1. $M = (40\,mg/mL) \times 50\,mL = 2.0\,gr$

2. $V_{ZrO_2} = \frac{2.0\,gr}{1.26\,gr/mL} = 1.59\,mL$

3. $V_{H_2O} = 50\,mL - 1.59\,mL = 48.41 mL$

Vita

Rosidian Aprillya Endang Palupi Esti Rahayu Widyastuti was born in Jakarta, Indonesia on April 14, 1972. She received her Bachelor of Science degree in Materials Science and Engineering from Arizona State University in December 1995. She joined the Fiber and Electro-Optic Research Center in May 1997 where she worked as a graduate research assistant. Aprillya received her Master of Science degree from the Materials Science and Engineering department in May 1998.

Aprillya is a member of the Society of Women Engineers and the National Society of Black Engineers. Her non-academic interests include sewing, baking, and different sports such as rockclimbing, rollerblading, golf, and racketball.